

Summary Report for the Development of Materials for Volatile Radionuclides

Advanced Fuel Cycle Initiative

***Prepared for
U.S. Department of Energy
Waste Forms
DM Strachan, J Chun,
CR Henager, Jr., J Matyáš,
BJ Riley, JV Ryan, PK
Thallapally
National Laboratories
August 2010
FCRD-WAST-2010-000189
PNNL- 20007***



DISCLAIMER

This information was prepared as an account of work sponsored by an agency of the U.S. Government. Neither the U.S. Government nor any agency thereof, nor any of their employees, makes any warranty, expressed or implied, or assumes any legal liability or responsibility for the accuracy, completeness, or usefulness, of any information, apparatus, product, or process disclosed, or represents that its use would not infringe privately owned rights. References herein to any specific commercial product, process, or service by trade name, trade mark, manufacturer, or otherwise, does not necessarily constitute or imply its endorsement, recommendation, or favoring by the U.S. Government or any agency thereof. The views and opinions of authors expressed herein do not necessarily state or reflect those of the U.S. Government or any agency thereof.

SUMMARY

The materials development summarized here is in support of the Waste Forms campaign, Volatile Radionuclide task. Specifically, materials are being developed for the removal and immobilization of iodine and krypton, specifically ^{129}I and ^{85}Kr .

During FY 2010, aerogel materials were investigated for removal and immobilization of ^{129}I . Two aerogel formulations were investigated, one based on silica aerogels and the second on chalcogen-based aerogels (i.e., chalcogels). For ^{85}Kr , metal organic framework (MOF) structures were investigated.

CONTENTS

<u>SUMMARY</u>	iii
<u>ACRONYMS</u>	ix
<u>1. INTRODUCTION</u>	1
<u>1.1 Aerogels</u>	1
<u>1.1.1 Functionalized Silica Aerogels for Off-gas Capture and Immobilization of ¹²⁹I</u>	1
<u>1.1.2 Chalcogen-Based Aerogels, or Chalcogels, for Iodine Sorbents</u>	5
<u>2. Metal Organic Frameworks for Xe and Kr immobilization</u>	13
<u>2.1 Key Personnel</u>	13
<u>2.2 Synthesis and Characterization of MOF-5 (BDCZn):</u>	13
<u>2.3 Synthesis and Characterization of DHTANi:</u>	15
<u>2.4 Xenon and Kr measurements using HPVA-100 and IGA-100</u>	16
<u>2.5 Air Stable Zeolitic Imidazolate Framework (ZIF) for Kr Immobilization:</u>	16
<u>2.6 Conclusions and Future Studies</u>	17
<u>3. Silicon Carbide for Gaseous Radionuclide Immobilization</u>	19
<u>3.1 Key Personnel</u>	19
<u>3.2 Background</u>	19
<u>3.3 Experimental Methods and Materials</u>	20
<u>3.4 Results</u>	21
<u>3.5 Future Work</u>	22
<u>4. References</u>	24

FIGURES

Figure 1. Formation of silver nanoparticles on silica aerogel surfaces.....	2
Figure 2. TEM image of Ag-functionalized aerogel (silver nanoparticles are black dots).....	2
Figure 3. Mass losses of raw and thiol-aerogels as determined with TGA.....	2
Figure 4. TGA-DSC curves for Ag-impregnated and reduced aerogels.....	3
Figure 5. Experimental setup for determining the maximum sorption capacity of functionalized silica aerogels.....	3
Figure 6. TGA-DSC curves for iodine-loaded aerogel.....	4
Figure 7. Schematic diagram of the experimental set-up for iodine uptake test in air containing 4.2 ppm I ₂	4
Figure 8. Schematic showing how the chalcogel is made and the iodine adsorption in the chalcogel network (modified from Brock) (Brock 2007).....	5
Figure 9. X-ray diffraction patterns for (A) (TMA) ₄ Ge ₄ S ₁₀ and (B) (TMA) ₄ Ge ₄ Se ₁₀ , the difference being the chalcogen atom used.....	7
Figure 10. Gelation of Ge-S-Pt gel in Petri dish or “P” casting.....	8
Figure 11. X-ray diffraction of (A) Cg-2P and Cg-3P showing amorphous structure with minor diffraction peaks matching Ge (PDF#72-1089, (Kasper and Richards 1964) open boxes) and GeO ₂ (PDF#34-1089, (Liu, Bassett and Sharry 1978) open circles). (B) Aged Cg-5P, Cg-5P + iodine, and a standard powder diffraction pattern for GeO ₂ (PDF# 85-0473). (Smith and Isaacs 1964).....	9
Figure 12. (A) Iodine sorption experiment (showing low packing density) and (B) results of iodine capture in terms of % of Total iodine (from calibration run) and measured iodine concentration in the scrubber solution (µg/L).....	10
Figure 13. Iodine sorption by mass% for both P- and C-method casted gels (P = plate-casted, C = cylindrical-casted).....	10
Figure 14. Thermogravimetric analysis (TGA) on (A) Cg-7C and (B) Cg-5C+I (with ~38–41 mass% iodine).....	11
Figure 15. (A) Precursors, i.e., Ni(NO ₃) ₂ ·6H ₂ O, CoCl ₂ ·6H ₂ O, and (NH ₄) ₂ (Mo,W)S ₄ , before and after mixing and after casted for a MoCo _{0.5} Ni _{0.5} S ₄ chalcogel. (B) The same gel as a hydrogel (prior to supercritical drying) suspended in H ₂ O.....	12
Figure 16. Metal-organic frameworks with different pore diameters (Rosi et al. 2003).....	13
Figure 17. Synthesis and single crystal X-ray structure of MOF-5.....	13
Figure 18. Thermal analysis of as synthesized MOF-5 and DMF exchanged with chloroform.....	14
Figure 19. In-situ Powder X-ray diffraction of MOF-5 at room 25°C and 200°C under vacuum.....	14
Figure 20. Synthesis and structural topology of DHTANi.....	15
Figure 21. TG-MS and BET surface area measurements on DHTANi.....	15
Figure 22. High pressure volumetric gas analyzer (HPVA-100, Left) and low pressure gravimetric gas analyzer coupled with MS and Breakthrough reactor (IGA-100, Right).....	16

Figure 23. Xenon and Kr adsorption (Δ) and desorption (∇) kinetics in MOF-5 (Left) and DHTANi (Right) at 25°C. 17

Figure 24. Structural stability of ZIF-8 under vacuum and air. 17

Figure 25. Metal Organic Frameworks suitable for Iodine adsorption. 18

Figure 26. Initial ion gun deposition setup for SiC immobilization experiments with Kr. 21

Figure 27. X-ray photoelectron spectra of the Kr 3d region showing Kr immobilized in sputtered SiC. This sample exhibited the maximum retention of 6.7 atomic % Kr (21.6 mass %). 22

Figure 28. Unbalanced magnetron setup used for several Kr immobilization experiments. 23

Figure 29. Peabody Scientific Ion Implanter System with beam energy: 2 to 40 keV via a Duoplasmatron Ion Source and low-pressure arc discharge system. 23

TABLES

Table 1. Summary of Ge-S-Pt gel preparation methods and properties ¹	8
Table 2. Experimental Setup for the SiC experiments.	21

ACRONYMS

AgZ	silver-loaded zeolite
BET	Brunauer, Emmett, Teller (a method of determining surface areas accessible to a gas
C	Cylindrical casting method
CFR	Code of Federal Register
Cg	chalcogel (sample identification prefix for chalcogels)
DF	decontamination factor
DSC	differential scanning calorimetry
EDS	energy dispersive spectroscopy
EPA	Environmental Protection Agency
FY	fiscal year
HSAB	Hard/Soft Acid-Base
ICP-MS	inductively coupled plasma – mass spectrometer
MOF	metal organic framework
MOF	metal-organic framework
PCT	Product Consistency Test
PDF	powder diffraction file
PNNL	Pacific Northwest National Laboratory
SEM	scanning electron microscopy
TEM	transmission electron microscopy
TGA-DSC	thermogravimetric analysis
TMA	tetramethyl ammonium
ZIF	zeolitic imidazolate frameworks

WASTE MANAGEMENT CAMPAIGN

1. INTRODUCTION

In his summary waste forms document, Gombert (2007) discussed many waste forms for the immobilization of volatile radionuclides. This list was narrowed in FY 2009 (Strachan et al. 2009). Here the continuation of the work discussed by Strachan (2009). Two types of aerogels, i.e., silica-based and chalcogen-based, were investigated as candidate waste forms for iodine immobilization. Metal organic frameworks and silicon carbide were investigated as candidate waste forms for ^{85}Kr immobilization, while metal organic frameworks were also looked at for ^{85}Kr removal. The methods, results, and conclusions of these studies in FY2010 are presented here.

1.1 Aerogels

Because of the long half-life, i.e., 1.6×10^7 y, wastes containing ^{129}I must be immobilized for hundreds of thousands of years. The EPA regulation 40 CFR 190 requires an ^{129}I capture decontamination factor (DF) of roughly 200 or more than 99% captured and immobilized. To support the future expansion of nuclear energy, an effective method is needed for the capture and safe storage of radiological ^{129}I released during reprocessing of spent nuclear fuel. Various materials have been investigated for the capture and immobilization of iodine. In most cases, however, the materials effective for capturing iodine cannot subsequently be sintered and densified to create a stable composite that is a viable waste form. The current material for capture of ^{129}I and the waste form is a silver-loaded zeolite (AgZ). In the work reported here, two types of aerogels are discussed as a potential replacement for the AgZ for ^{129}I capture and immobilization: silica aerogels and chalcogen-based aerogels, termed chalcogels.

1.1.1 Functionalized Silica Aerogels for Off-gas Capture and Immobilization of ^{129}I

1.1.1.1 Key Personnel

J Matyáš, G. Fryxell, K. Wallace, and L. Fifield

1.1.1.2 Summary

Experiments during the first year of the project demonstrated that it is possible to functionalize aerogels to make them effective for capturing of iodine, and that, once laden with iodine, the aerogels can be sintered and densified, creating a viable waste form. The maximum sorption capacities of functionalize aerogels were found to be ~ 200 mg I_2/g at 115°C . Approximately 92 mass% I_2 was retained in densified aerogels after thermal sintering with mild pressure at 1200°C for 30 min.

The primary objectives of this year were to further improve the maximum sorption capacities of silver-loaded aerogels for iodine and to demonstrate their high sorption efficiency in the gas stream containing low concentrations of I_2 . These objectives were successfully met. The partially optimized aerogels showed maximum sorption capacity of more than 558 mg I_2/g at 150°C . The iodine uptake test with air containing 4.2 ppm I_2 showed no I_2 breakthrough after 3.5 h and indicated a decontamination factor (DF) in excess of 310. In addition, we have showed than 93.8 mass% I_2 can be retained in the aerogel after densification at 1300°C for 15 min.

1.1.1.3 Functionalization of silica aerogel surfaces

The surfaces of free-standing aerogels from United Nuclear were chemically modified with the supercritical fluid chemistry previously developed at PNNL (US Patent #7,019,037 2006). This procedure is both fast and efficient, and produces very little waste. These materials are produced with a process that is similar to a PNNL technology has been licensed and is currently being used for commercial production.

The formation of silver nanoparticles on silica aerogel surfaces is schematically described in Figure 1. The hydroetched and hydrated granules of silica aerogel were functionalized with the deposition of a propylthiol monolayer on the surface by treating the aerogel with 3-mercaptopropyltrimethoxysilane in supercritical CO₂ solvent (~7500 psi and 150°C). Silver ions were reacted with the thiol monolayer interface by treatment with ~200 mL of 3.25 mass% AgNO₃ solution, thereby forming a layer of Ag(I) ions.

About 25 mL of isopropanol was added to the solution to enable wetting of the moderately hydrophobic thiol-modified aerogel, which led to complete dispersability of aerogel granules. The silver nanoparticles were produced on the silica aerogel surfaces through reduction of silver ions at 165°C for 2h under flowing 2.7% H₂ in Ar.

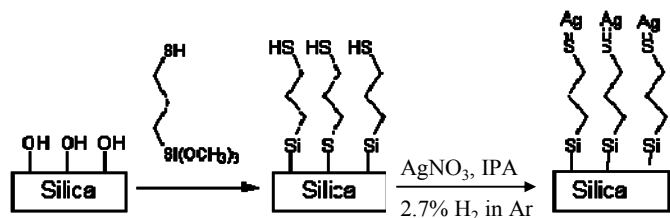


Figure 1. Formation of silver nanoparticles on silica aerogel surfaces.

The high degree of surface functionalization was demonstrated and characterized with Brunauer, Emmett, Teller (BET) analysis, simultaneous thermogravimetry and differential scanning calorimetry (TGA-DSC), and transmission electron microscopy (TEM). The BET surface areas decreased from 818 m²/g for raw aerogel to 620 m²/g for thiol-aerogel and to 199.1 m²/g for Ag-functionalized aerogel. The pore volume followed the same trend and decreased from 5.4 to 3.5, and 0.18 cm³/g, respectively, confirming a good surface coating with functionalized groups. Analyses in the TEM revealed uniform distribution and size of silver nanoparticles (< 10 nm) on the surfaces of highly porous silica aerogel (Figure 2).

Figure 3 shows TGA curves for raw and thiol-aerogels. Raw aerogel exhibited two distinct mass losses during the heating. First, ~2 mass% of physically adsorbed water was lost at temperatures below 100°C, and then ~9 mass% of silanol groups gradually disappeared at temperatures above 350°C. For thiol-aerogel, an initial 0.4 mass% loss at 25-50°C was attributed to the water physically adsorbed on the surface. The mass loss ~41 mass% at 50 – 530°C was the decomposition of the thiol moiety that was anchored on the aerogel surfaces. The mass loss 2.5 mass% at temperatures above 530°C corresponded to removal of the remaining silanol groups. Figure 4 shows TGA-DSC curves for two aerogels, Ag-impregnated (aerogel after treatment with AgNO₃) and silver-reduced (aerogel after reduction under H₂/Ar). Both aerogels showed ~8 mass% loss at temperature range from 265°C to 400°C from the decomposition of residual unreacted AgNO₃ that remained physically absorbed inside the aerogel structure.

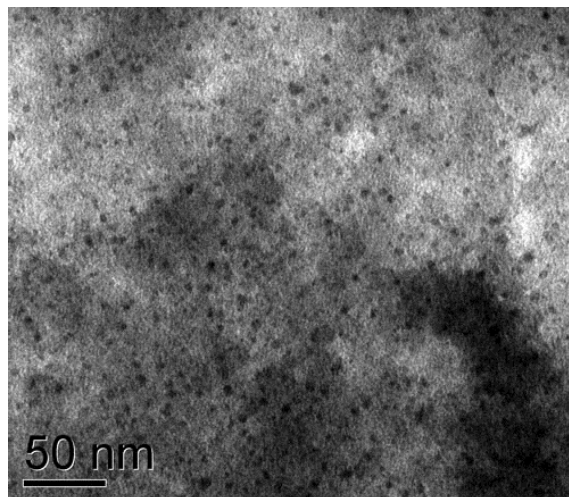


Figure 2. TEM image of Ag-functionalized aerogel (silver nanoparticles are black dots).

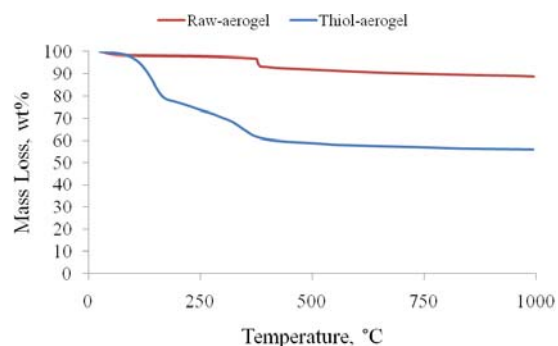


Figure 3. Mass losses of raw and thiol-aerogels as determined with TGA.

1.1.1.4 Iodine uptake test in the absence of carrier gas

Figure 5 shows the experimental setup that was designed and assembled to determine the maximum sorption capacity of functionalized silica aerogel for iodine. Teflon vessel with ~1g of solid I₂ was connected to the column with sorbent and heated in the oven to 150°C. The I₂ gas was allowed to pass through the column with a sorbent to the beaker containing 1M NaOH over the period of 24 h. To remove the loosely bonded or excess of iodine, the column was detached, heat-treated in another oven at 150°C overnight, and transferred into vacuum desiccator for 24h. Subsequently, the column was removed from desiccator and weighed to obtain the mass gain (sorption capacity mg I₂/g) of Ag-impregnated aerogel. The sample gained 55.9 mass%. The TGA-DSC was used to verify the high sorption capacity of I₂-loaded functionalized aerogel. Figure 6 shows the mass loss and mass-corrected heat flow as a function of temperature. The total sample mass lost was 56.8 mass%, including ~1 mass% of physically absorbed water. Therefore, 55.8 mass% corresponds to captured I₂, of which 11.5 mass% can be attributed to reaction of residual AgNO₃ with iodine and to release of physically sorbed iodine. The majority, 44.3 mass% loss, comes from the decomposition of silver iodide that starts at 558°C and corresponds to maximum sorption capacity of aerogel for iodine.

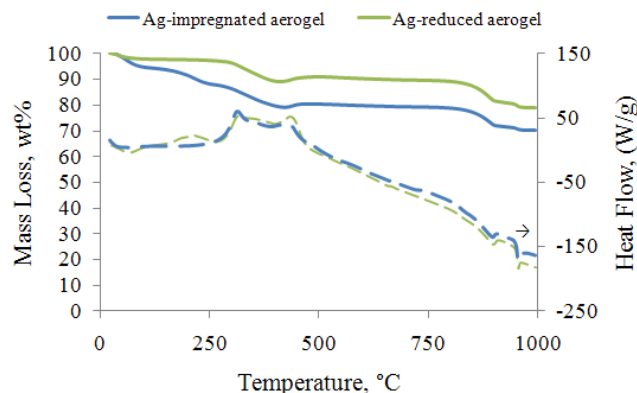


Figure 4. TGA-DSC curves for Ag-impregnated and reduced aerogels.

1.1.1.5 Iodine uptake test in air containing 4.2 ppm of iodine

Figure 4 shows a schematic diagram of the experimental set-up. Air (67 ppm H₂O) was allowed to pass through the U-tube containing glass beads and iodine permeation tube. The 4.2 ppm of iodine in the carrier gas was established by heating the permeation tube in the oven to 100°C and adjusting the carrier gas flow rate to 18.9 mL/min (carrier gas linear velocity 0.0401 m/s). Two independent 1-h long calibration runs (no sorbent present in the column) were performed to confirm the concentration of iodine in the carrier gas. Concentrations of I₂ in the solutions were 2468 and 2495 µg/L and agreed well with 4.2 ppm of iodine in the carrier gas. The air with iodine was allowed to pass through the column with ~0.5 g of Ag-reduced aerogel heated in the oven to 150°C to the beaker containing 20 mL of 0.1M NaOH. The beaker

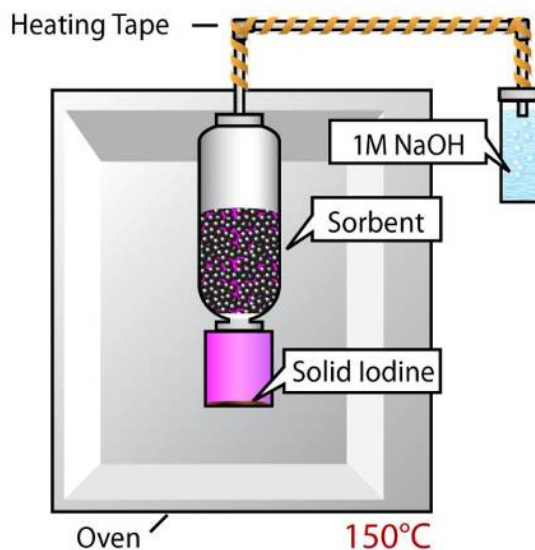


Figure 5. Experimental setup for determining the maximum sorption capacity of functionalized silica aerogels.

with caustic solution was replaced every 30 min. The NaOH solutions were analyzed for I_2 with ICP-MS (detection limit $\sim 4 \mu\text{g}$ of iodine /L). For aerogel, there was no I_2 present in the analyzed solutions, indicating 100% capture efficiency and $DF > 310$. About $175 \mu\text{g}$ of I_2 was removed out of $175 \mu\text{g}$ possible.

1.1.1.6 Immobilization of iodine-loaded silica aerogel

Raw, silver-reduced and iodine-loaded silica aerogels were ground with mortar and pestle, and pressed into a pellet at 32 MPa. Three pellets were prepared. The first pellet contained 0.099 g silver-reduced aerogel, the second 0.0835 g silver-reduced aerogel and 0.0204 g raw aerogel, and the third 0.0764 g iodine-loaded aerogel and 0.0185 g raw aerogel. The pellets were transferred onto 25×25 mm Pt sheets and heat-treated at 1300°C for 15 min. The air-quenched pellets were stored in the desiccator for an hour under vacuum before being weighted. From the mass losses, we were able to estimate the retention of iodine in the final product. Mass loss results indicated that 93.8 mass% of iodine was retained in densified aerogels for loadings ~ 558 mg of I_2 per gram, suggesting that silver nanoparticles that were produced through functionalization of silica aerogel surfaces retained all the iodine (443 mg of I_2 per gram). The remaining I_2 (~ 80 mg of I_2 per gram) is probably retained by AgI that was produced by reaction of the residual AgNO_3 and I_2 . The ICP-MS results for the densified iodine-loaded aerogel are pending and were not available before finalizing this report.

1.1.1.7 Conclusions

We were able to more than double the maximum sorption capacities of functionalized silica aerogels for iodine relative to our FY2009 materials and demonstrated their high sorption efficiency in the gas stream containing low concentrations of iodine. Functionalized aerogels showed maximum sorption capacities of 558 mg of I_2 per gram and DFs higher than 310 at 150°C .

Preliminary densification experiments showed high retention, ~ 94 mass% iodine, after 15 min at 1300°C .

1.1.1.8 Future Work

Next year, we would like to further improve the capture efficiencies of functionalized aerogels for iodine as well as retention of iodine in densified aerogels. In addition, we will investigate chemical durability of the densified aerogels with the Product Consistency Test (PCT).

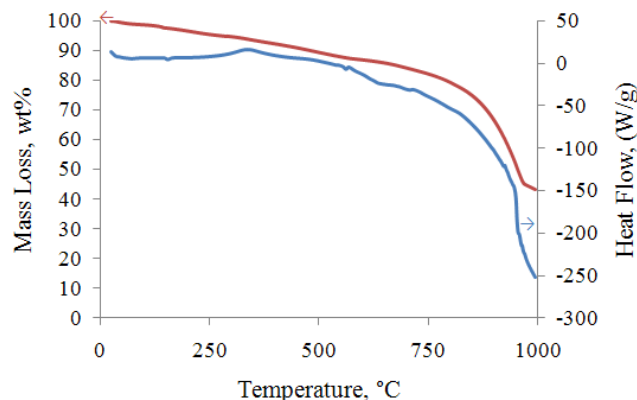


Figure 6. TGA-DSC curves for iodine-loaded aerogel.

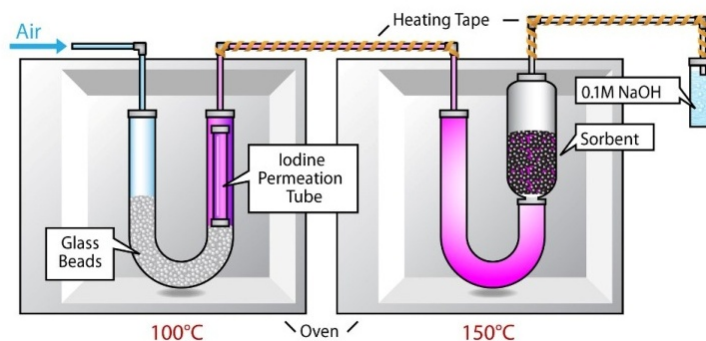


Figure 7. Schematic diagram of the experimental set-up for iodine uptake test in air containing $4.2 \text{ ppm } I_2$.

1.1.2 Chalcogen-Based Aerogels, or Chalcogels, for Iodine Sorbents

1.1.2.1 Key Personnel

Key Investigators: Brian Riley, Jaehun Chun, Joseph Ryan

Key Contributors: Dean Matson, Xiaohong (Shari) Li, Josef Matyas

1.1.2.2 Background

This work is focused on an ^{129}I waste form made from chalcogels – aerogels containing metal and chalcogenide (i.e., S, Se, and/or Te) atoms. Better thermal stability and efficiency of the chalcogel-based waste form are expected from stronger complex formations over AgZ: a stronger chemical affinity of chalcogenide atom with iodine gas. The stronger chemical affinity is due to the soft Lewis acid/soft Lewis base complex formation, according to Pearson's Hard/Soft Acid-Base (HSAB) principle (Pearson 1963).

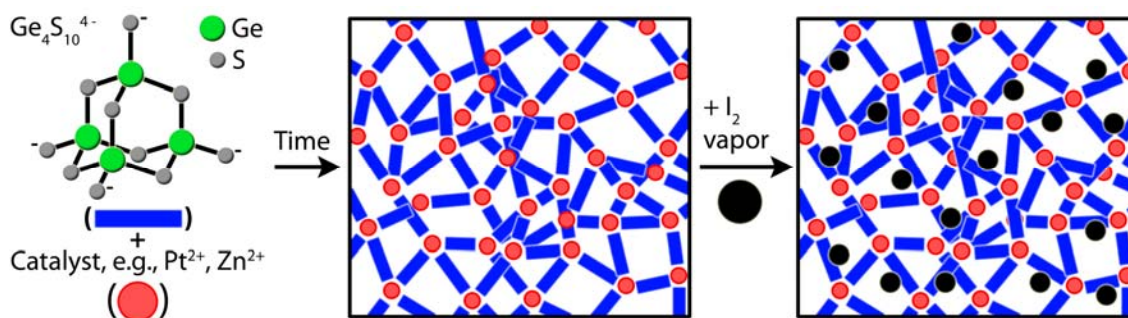


Figure 8. Schematic showing how the chalcogel is made and the iodine adsorption in the chalcogel network (modified from Brock) (Brock 2007).

As reported elsewhere (Ryan et al. 2009), we are using chalcogen-based semiconductor aerogels, or “chalcogels,” pioneered by Bag and Kanatzidis (2008; 2009; 2007; 2008) as iodine sorbents. Figure 8 is a schematic showing how to make a Ge-Ch-*c* gel, where Ch is a chalcogen atom and *c* is the catalyst interlinking the structural units, in this case, $\text{Ge}_4\text{S}_{10}^{4-}$ adamantine-like units. Figure 8 shows how iodine is adsorbed into the network of a Ge-S-*c* chalcogel. Bag and Kanatzidis demonstrated the wide compositional flexibility of these chalcogels in which the properties, i.e., surface area per unit mass (10–528 m^2/g) (Bag et al. 2009; Bag et al. 2007), band gap (2.0–0.8 eV) (Bag et al. 2007), selective affinity (i.e., liquids, vapors), etc., can be “tuned” by changing the metal and chalcogen precursors.

Initially, Bag and Kanatzidis used platinum as an interlinking agent for the $(\text{Ge},\text{Sn})_x\text{Ch}_y\text{-}c$ chalcogels (where building blocks are $\text{Ge}_4\text{S}_{10}^{4-}$, $\text{Ge}_4\text{Se}_{10}^{4-}$, $\text{Sn}_4\text{S}_{10}^{4-}$, $\text{Sn}_2\text{Se}_6^{4-}$, SnS_4^{4-} , SnSe_4^{4-}), but found that route cost-prohibitive and, thus, they pursued a processing route, in which they utilized other interlinking metals, e.g. Zn, as well as other building blocks, e.g. $(\text{Mo},\text{W})\text{S}_4^{2-}$. Bag and Kanatzidis also demonstrated a wide variety of uses for these materials, in which they can be used as sorbents with selective affinity for heavy metals (e.g., Hg vs. Zn) (Bag et al. 2007) and selective sorbents or catalysts for gas separation, e.g. hydrodesulfurization (Bag et al. 2009), to name a few applications.

1.1.2.3 Chalcogel Properties

Some of the property parameters (e.g., durability) that are important waste form properties are not available in the literature for these types of aerogels, because of their relative recent discovery was only in 2007 (Bag et al. 2007). Therefore, many of their properties are estimated based on glasses that had similar chemistries.

1.1.2.3.1 **Currently Achievable Waste Loading**

Greater than 200 mass% is achievable from a saturated iodine environment at room temperature though the thermal stability of these gels is low at $T \geq 100^\circ\text{C}$.

1.1.2.3.2 **Achievable Density**

The supercritically-dried Ge-S-Pt chalcogel has a very low unpacked, bulk density of $< 500 \text{ kg/m}^3$. For amorphous Ge_4S_{10} , $\rho \sim 3 \times 10^3 \text{ kg/m}^3$, though with the addition of iodine ($\rho = 4.930 \times 10^3 \text{ kg/m}^3$, 20°C) (CRC Handbook of Chemistry and Physics 2007-2008) and with inclusion of Pt ($\rho = 21 \times 10^3 \text{ kg/m}^3$, 20°C) (CRC Handbook of Chemistry and Physics 2007-2008) in the structure, this will increase if collapsed to a zero porosity solid by melting. Also, other chalcogel chemistries (i.e., replace S with higher Z and ρ elements, Se and/or Te) will be explored in the future to further increase density.

1.1.2.3.3 **Durability**

Although performance assessment tests have not yet been performed, acceptable chemical durability is expected, based on limited durability data on chalcogalides. If the durability of the Ge-S aerogels is determined to be low, different chemistries are available to optimize the performance as chalcogenides form very forgiving networks. Typically, chalcogenide-based glasses are well known to be soluble in caustic environments (Riley et al. 2008).

1.1.2.3.4 **Temperature Stability**

Based on limited thermal analysis data in the literature on these types of aerogels (Bag et al. 2007), Ge-Ch-Pt chalcogels appear to be stable at $T \leq 550^\circ\text{C}$ where mass loss is observed to be decomposition, i.e., loss of sulfur (Bag et al. 2007). At this temperature, the adsorbed iodine (i.e., desorption) is assumed to be lost, although this remains. The glass transition temperature, T_g , of Ge-S glasses decreases with the addition of iodine (Kirilenko and Dembovskii 1975) and, therefore, the thermal stability of the aerogel is expected to be related to the waste loading, i.e. the higher iodine loading, the lower the thermal stability.

1.1.2.3.5 **Thermal Conductivity**

According to the literature, the thermal conductivity of a silica aerogel with surface area of $800 \text{ m}^2/\text{g}$ was reported as $0.036 \text{ W/m}\cdot\text{K}$ (Wei et al. 2007). Chalcogels are assumed to have similar thermal conductivities. The thermal conductivity of Ge-S glasses reported in the literature (Hilton and Hayes 1975) show values in the range of $\sim 0.3 \text{ W/m}\cdot\text{K}$.

1.1.2.4 **Methods & Results**

As discussed in earlier work (Ryan et al. 2009), many of the building blocks required are unavailable commercially. Thus, to make some of these chalcogels, we had to produce them in the laboratory. For Ge-S,Se chalcogels, Ge-S,Se precursors we used hydrothermal conditions. The following chemicals were reacted in a Teflon[®] crucible within a pressure vessel according to methods presented in the literature (Bowes et al. 1996): germanium powder (-100 mesh, 99.9999% purity, Alfa Aesar), sulfur (99.9999% purity, ASARCO) or selenium (99.9999% purity, Alfa Aesar) powder(s) (-100 mesh), tetramethyl ammonium hydroxide [(CH₃)₄NOH or (TMA)OH], and water in the mole ratios of 4, 10, 5, and 75–100, respectively. The reactants were stirred with a Teflon-coated, magnetic stir-bar, while the vessel was heated at $\sim 140^\circ\text{C}$ for ≥ 16 hours. Following the digestion, the solution was vacuum filtered and the filtrate collected. Ethanol and acetone were then added to the filtrate resulting in the precipitation of fine particles of (TMA)₄Ge₄(S,Se)₁₀ that were vacuum filtered and washed with ethanol and acetone. The resulting precipitates were dried under vacuum, ground to powder, and analyzed with XRD (Bruker D8 Advanced with a LinxEye detector) to verify the products. Both precipitates match the diffraction pattern for (TMA)₄Ge₄S₁₀ presented by Pivan *et al.* (PDF#52-7775) (see Figure 9) (Pivan et al. 1994).

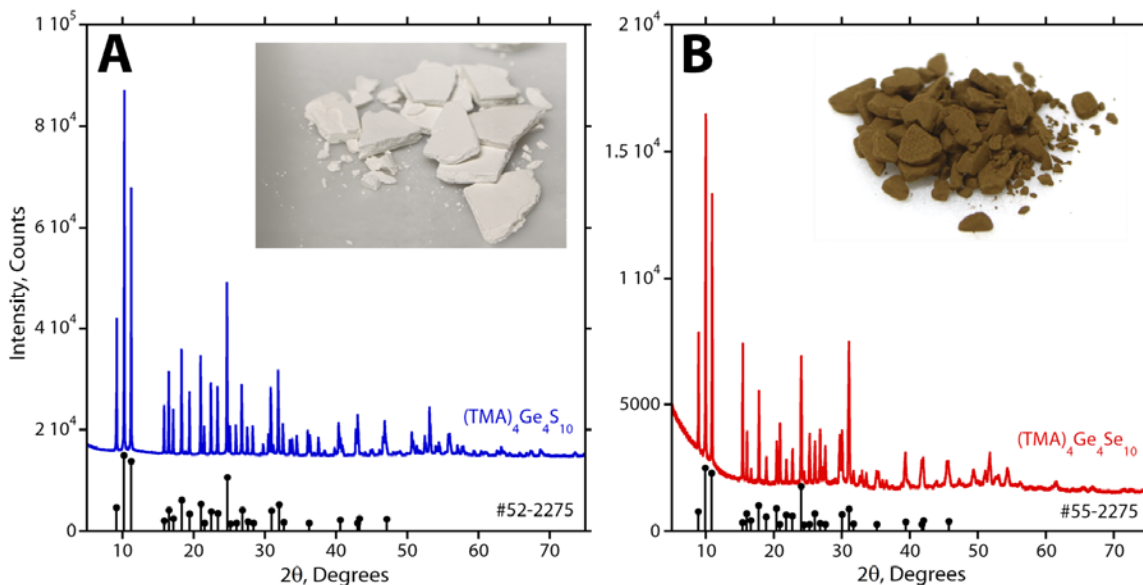


Figure 9. X-ray diffraction patterns for (A) $(\text{TMA})_4\text{Ge}_4\text{S}_{10}$ and (B) $(\text{TMA})_4\text{Ge}_4\text{Se}_{10}$, the difference being the chalcogen atom used.

Another precursor option for the Ge-Ch adamantine structures will be studied in FY2010 where Ag or Cu is substituted in for two of the TMA units yielding $(\text{TMA})_2(\text{Ag,Cu})_2\text{Ge}_4(\text{S,Se})_{10}$ as presented by Bowes *et al.* (1996). The Ag-based precursor is an attractive option in this instance because Ag has a high affinity for iodine. This precursor forms as a precipitate from a solution of sodium thiosulfate, silver nitrate, and $(\text{TMA})_4\text{Ge}_4(\text{S,Se})_{10}$. Bowes *et al.* (1996) described the process for the $(\text{TMA})_4\text{Ge}_4\text{S}_{10}$ precursor but it can be extrapolated to the $(\text{TMA})_4\text{Ge}_4\text{Se}_{10}$ precursor. To make these Ag,Cu precursors, solution 1 is made up of two separately prepared sub-solutions: a 1-g solution of 0.1044 g $\text{Na}_2\text{S}_2\text{O}_3$ (0.66 mmol) and a 1-g solution of 0.03737 g AgNO_3 (mass balance is H_2O) that are made up separately and then mixed together. Solution 2 is made by dissolving 0.1997 g or 0.3029 g of $(\text{TMA})_4\text{Ge}_4\text{S}_{10}$ or of $(\text{TMA})_4\text{Ge}_4\text{Se}_{10}$, respectively, (0.22 mM). The two solutions are then mixed together and left to sit for 16 hr at room temperature.

1.1.2.5 Ge-S-Pt Chalcogel Improvements

Germanium-S-Pt chalcogels were successfully made in FY2009 (Ryan *et al.* 2009) and in FY2010, the PNNL team was successful in modifying the gelation process to increase Brunauer Emmett Teller (BET) surface area of the gels. In FY2010, we conducted iodine gas adsorption tests (in saturated and diluted-stream conditions) as well as characterization of the chalcogel (e.g., surface area, pore sizes, and pore distribution) with and without iodine. Table 1 summarizes the results from the primary chalcogels studied in FY2010 for which surface area, pore volume, and pore size were measured. These include: Cg-5C, Cg-5P and -5P + iodine, Cg-6C, and Cg-7C, for which the casting method, the gelation time, and aging time were varied (“Cg” for chalcogel).

If the chalcogel solution was exposed to air during gelation, i.e., while in a Petri dish as was done by Bag *et al.* (2008; 2009; 2007) and the PNNL team in FY2009 (Ryan *et al.* 2009), the gel turned very dark in appearance (optically opaque) after ~24–48 h as seen in Figure 10. Being that these are non-oxide semiconducting materials, these chalcogels were assumed to be light- and/or oxygen-sensitive. The method of casting the gels in a Petri dish was termed the “Plate” or “P” casting method and the surface areas of gels cast with this method were consistent (but slightly lower) with those reported in the

Table 1. Summary of Ge-S-Pt gel preparation methods and properties¹.

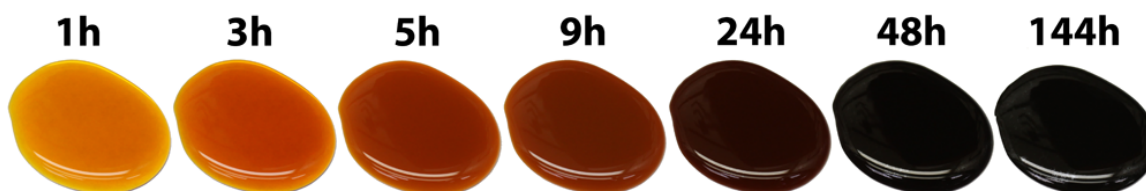
Sample Id	Gelation time, d	Aging time, d	Degas T , °C	S , m ² /g	Pore vol., 10 ⁶ m ³ /g	Pore size, nm	Pore size peak, nm
Cg-5C	6	2	25	360	2.3	20-150	-
			60	342	2.15	20-150	-
			100	387	2.38	20-150	-
Cg-5P	6	2	25	287	1.62	20-150	-
			60	271	1.34	20-150	-
			100	252	1.44	20-150	-
Cg-5P+I	6	2	25	48.6	0.32	20-150	-
			60	83.2	-	-	-
			100	77.6	0.49	20-150	-
			125	66.3	0.43	20-150	-
Cg-6C	17	8	25	416.5	2.03	20-150	-
			60	399.0	-	-	-
			100	383.4	2.35	20-150	-
			125	355.1	2.08	20-150	-
Cg-7C	18	8	25	423	3.1	20-150	35
			60	491	3.4	20-150	65
			100	418	2.9	20-150	70
			125	428	3.0	20-150	50

1) “Degas T ” is the temperature in °C that the specimen was heated at prior to taking BET measurements. “ S ” refers to the measured BET surface area in m²/g. “Pore vol.” refers to the measured BET pore volume in 10⁶ m³/g. “Pore size” is the measured BET pore size and sometimes a maximum value was listed (“Pore size peak”)

literature, i.e., 252–287 m²/g (i.e., 252, 271, and 287 m²/g at temperatures of 100, 60, and 25°C, respectively) for our Ge-S-Pt gels versus the literature values of 276–323 m²/g (at 25°C) (Bag et al. 2007; Kanatzidis and Bag 2008). See Table 1 for more details.

Thus, to improve the gelation process and hopefully improve the properties of the gels, we experimented with casting in polymer vials with zero headspace and wrapping the casted vials in aluminum foil to prevent minimize the exposure of the gels to oxygen and light, respectively. This casting technique, termed the “*Cylindrical*” or “*C*” casting method, yielded gels with a color similar to that of the 9-h gelation time gel when casted in the Petri dish (Figure 10), a much lighter shade of brown and much higher surface area, up to 491 m²/g, after a degas at 60°C. This surface area is to be compared to literature values of ~ 300 m²/g after degassing at 75°C (Bag, Arachchige and Kanatzidis 2008; Bag et al. 2007; Kanatzidis and Bag 2008).

The elements used to prepare chalcogels are much heavier than those for silica aerogels, which makes a direct comparison of specific surface areas unreasonable. In order to compare the surface areas of these chalcogels with those of the silica aerogels, Bag et al. presented a *SiO₂ equivalent* which is simply a way of normalizing the chalcogel composition to two anion, i.e., chalcogen, atoms, Pt_{0.4}Ge_{0.8}S₂ (for Pt₂Ge₄S₁₀

**Figure 10.** Gelation of Ge-S-Pt gel in Petri dish or “*P*” casting.

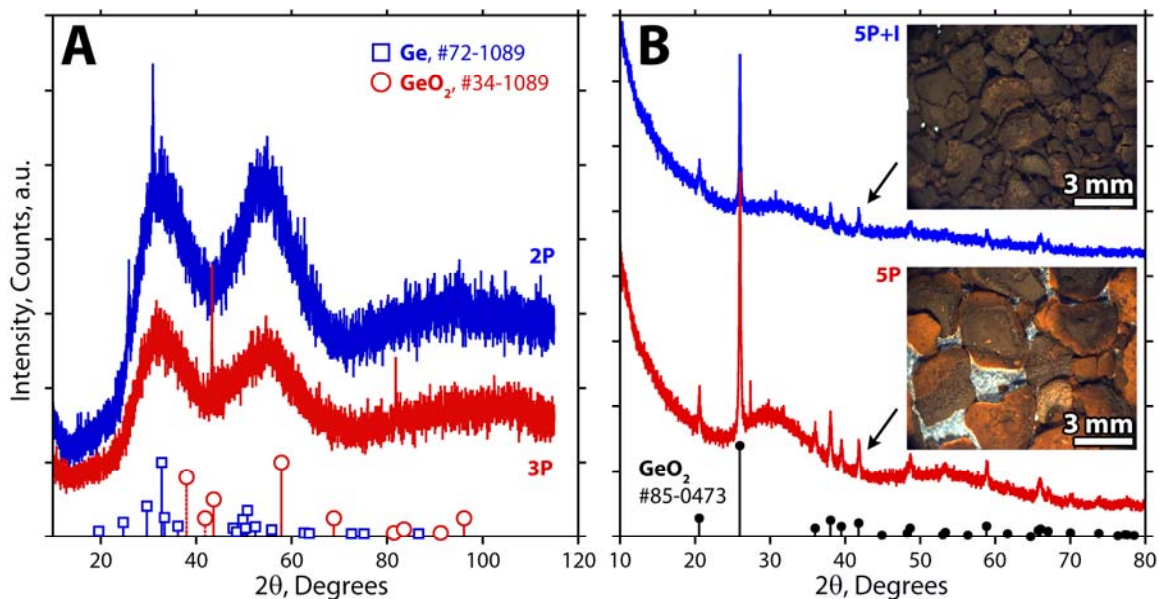


Figure 11. X-ray diffraction of (A) Cg-2P and Cg-3P showing amorphous structure with minor diffraction peaks matching Ge (PDF#72-1089, (Kasper and Richards 1964) open boxes) and GeO₂ (PDF#34-1089, (Liu, Bassett and Sharry 1978) open circles). (B) Aged Cg-5P, Cg-5P + iodine, and a standard powder diffraction pattern for GeO₂ (PDF# 85-0473). (Smith and Isaacs 1964)

chalcogel) as compared to SiO₂. With this method, we calculated the *SiO₂ equivalent* is > 1636 m²/g for the chalcogel with 491 m²/g.

Gels from PNNL's FY2009 work, i.e., Cg-2P and -3P, were analyzed with XRD. The gel was nearly completely amorphous as seen in Figure 11-A with the exception of a few diffraction peaks which best fit to Ge and GeO₂ (Kasper and Richards 1964; Liu, Bassett and Sharry 1978). Figure 11-A is a representative diffraction pattern for gels casted using the "P" method in FY2009, analyzed closely following supercritical drying and are comparable those presented in the literature (Bag et al. 2007; Kanatzidis and Bag 2008).

Samples Cg-5P and Cg-5P+I were prepared for XRD analysis after being in a vacuum desiccator for several months following the completion of gelation and iodine sorption experiments. The gels were suspended in ethanol within small glass vessels where they were crushed to a fine powder and then dropped onto zero-background silicon wafer XRD sample holders. The ethanol for the Cg-5P+I specimen became noticeably yellow suggesting that some of the iodine was removed in the suspension process. The diffraction peaks observed by XRD match those of GeO₂ (PDF# 85-0473) suggesting that the darker color of aged Ge-S-Pt chalcogels can be attributed to the oxidation of germanium to GeO₂ – see Figure 10 and Figure 11-B. In Figure 10, the color gradient from a bright orange to a dark brown/black of Cg-5P can be seen clearly. This gradient is caused by air exposure of part of the gel during the aging and solvent exchanges processes. The PNNL team believes that gel oxidation can be eliminated with careful precautions to reduce gel exposure to oxygen and light during gel production.

1.1.2.6 Iodine Uptake Experiments

In order to determine the maximum sorption of the chalcogels for iodine, two different types of chalcogels were analyzed: Cg-5C and Cg-5P. Here, each specimen was loaded into a separate pre-weighed glass scintillation vials and loaded into a vacuum desiccator with pure iodine metal (Alfa Aesar, 99.9999% purity) at a pressure of 1.3–6.7 Pa (10–50 mTorr) and taken out regularly for mass

measurements. Initial masses of the Cg-5C and Cg-5P were 0.0465 g and 0.1032 g, respectively. Sample Cg-5C showed an uptake of ~200% by mass of iodine after 4 days in the vacuum desiccator and > 240% by mass after 3 weeks (Figure 13). This value was higher than that of Cg-5P, an effect that we attributed to higher surface areas measured for Cg-5C (360 g/m² for 5C versus 287 g/m² for 5P at 25°C, see Table 1). Following the adsorption, the gels were left in the desiccator under vacuum to observe the iodine desorption; some of the iodine was desorbed over time though the rate of desorption was very low compared to the rate of adsorption and appeared to be linear over the course of ~25 days (Figure 13). Following the iodine saturation experiment, the Cg-5P+I gel was analyzed with BET

and the surface area was recorded at 25°C to be 48.6 m²/g (compared to 287 m²/g for Cg-5P) and the pore volume of 3.2×10⁻⁷ m³/g (compared to 1.6×10⁻⁶ m³/g in Cg-5P), both a large decrease from Chalcogel-5P.

A separate iodine sorption test was performed in low iodine concentrations and elevated temperatures (~140°C) which is closer to a simulated waste stream environment than an idealized, saturated iodine atmosphere. A stream of dry air passed through iodine using a DYNACAL[®] iodine permeation tube with a permeation rate of 1371.58 ng/min yielded a concentration of 4.2 ppm by volume. The pipette with Chalcogel-7C was inserted into the line of iodine vapor where the gas entered from the bottom of the pipette near the disc and exited through the top and the exit gas was scrubbed in 0.1 M NaOH solutions which were changed out every 30 minutes. A blank run was made without the chalcogel where the iodine concentration was measured in the scrubber solution after 30 and 60 minutes. The measured concentrations were 1234 and 2495 µg/L, respectively, which provided a calculated value of 41.49 µg/L/min of iodine according to a linear fit to the calibration data.

For this experiment, 0.0666 g of Chalcogel-7C was loaded into a 10 mL glass pipette lightly packed and held vertical by a porous Al₂O₃ disc (see Figure 13-A). The 0.1 M NaOH scrubber solutions were removed at 21.3, 183,

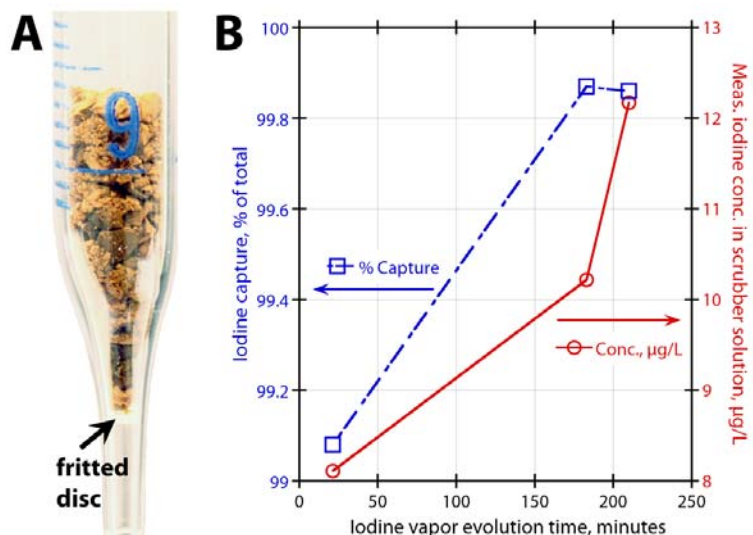


Figure 12. (A) Iodine sorption experiment (showing low packing density) and (B) results of iodine capture in terms of % of Total iodine (from calibration run) and measured iodine concentration in the scrubber solution (µg/L).

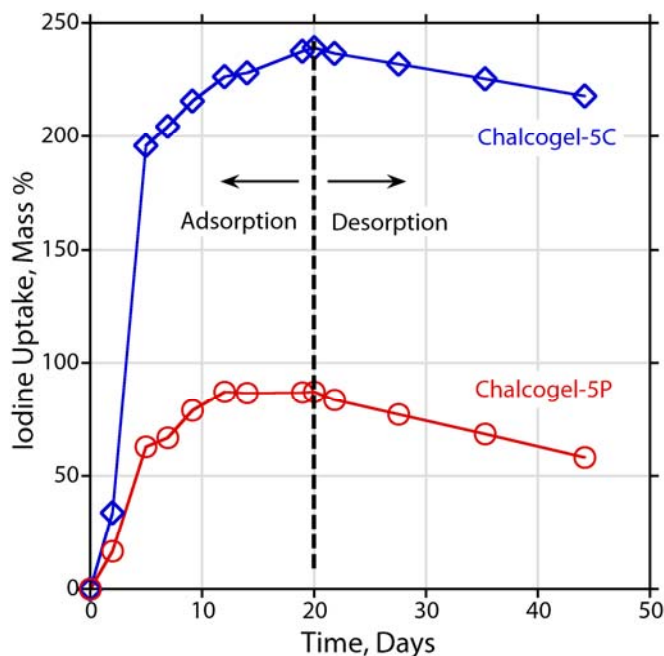


Figure 13. Iodine sorption by mass% for both *P*- and *C*-method casted gels (*P* = plate-casted, *C* = cylindrical-casted).

and 210 minutes of the sorption process and were analyzed by inductively coupled plasma mass spectrometry (ICP-MS). Following the experiment, the pipette was weighed and the final mass increase was determined to be 0.0012g (1.80% increase, by mass). The chalcogels demonstrated >99% uptake at low packing density over the entire duration of the experiment – see Figure 12-B. Future experiments will be performed with powdered chalcogels instead of chunks of chalcogel to increase the surface area available for the iodine vapor.

1.1.2.7 Thermal Analysis

Samples Cg-7C and Cg-5C+I were analyzed with a Seiko thermogravimetric differential thermal analyzer. Prior to the analysis, the iodine content of Chalcogel-5C+I was verified with scanning electron microscopy energy dispersive spectroscopy (SEM-EDS) to be ~38–41 mass% (depending on the region analyzed). The specimens were heated from room temperature to 800°C at 5°C/min. The thermal profile for Cg-7C matched very closely to that presented by Bag *et al.* (2007) for their Ge-S-Pt chalcogel with a mass loss of 55–60 mass% after heating to 800°C. The iodine-sorbed chalcogel, Cg-5C+I showed a high rate of mass loss at $T \geq 100^\circ\text{C}$, which is attributed to the desorption of iodine and decomposition of the chalcogel though this is a worst-case scenario.

1.1.2.8 (Mo,W)S₄²⁺-Based Chalcogels

Bag *et al.* (2009) studied chalcogels which utilize (Mo,W)S₄²⁺ building units and do not include Pt²⁺ as an interlinker but rather other d²⁺ transition metals, i.e., Co, Ni. These materials actually have a higher chalcogen-to-metal, or Ch:M, ratio of 2:1 as compared with the 1.67:1 for the Ge-Pt-S compounds so that one may expect a better iodine capture. The precursors are all commercially available and include: (NH₄)₂(Mo,W)S₄, Ni(NO₃)₂·6H₂O, CoCl₂·6H₂O. A schematic of the gelation process is shown in Figure 15-A. These materials tend to gel more effectively than do the TMA-based gels and create a more coherent/rigid gel that is easier to handle (Figure 15-B). The only drawback is that the precursors are not water soluble but rather soluble in formamide, which has some chemical hazards though these are lower than the hazards associated with working with TMA-OH.

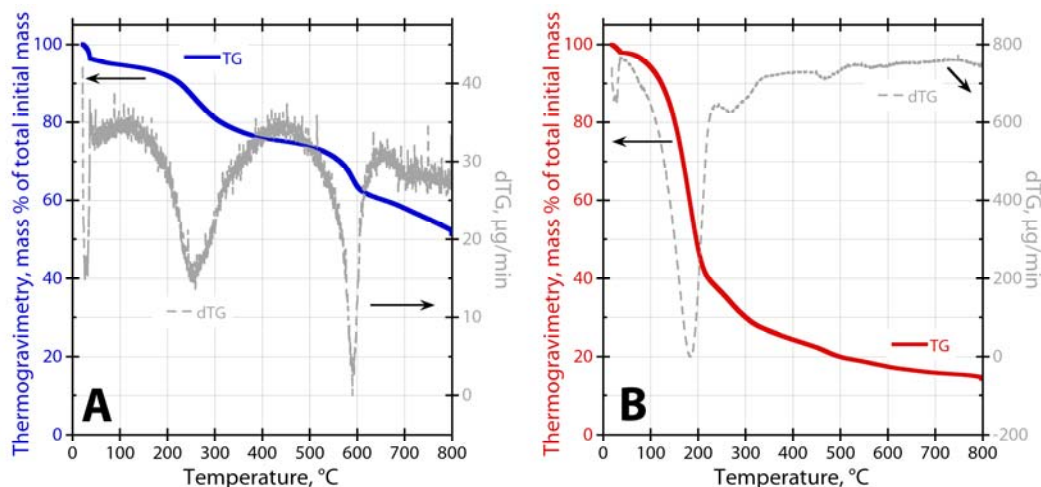


Figure 14. Thermogravimetric analysis (TGA) on (A) Cg-7C and (B) Cg-5C+I (with ~38–41 mass% iodine).



Figure 15. (A) Precursors, i.e., $\text{Ni}(\text{NO}_3)_2 \cdot 6\text{H}_2\text{O}$, $\text{CoCl}_2 \cdot 6\text{H}_2\text{O}$, and $(\text{NH}_4)_2(\text{Mo,W})\text{S}_4$, before and after mixing and after casted for a $\text{MoCo}_{0.5}\text{Ni}_{0.5}\text{S}_4$ chalcogel. (B) The same gel as a hydrogel (prior to supercritical drying) suspended in H_2O .

1.1.2.9 Summary of Results

Ge-S-Pt gels were successfully made and the surface areas significantly increased ($491 \text{ m}^2/\text{g}$) from chalcogels of the same chemistry reported in the literature ($\sim 300 \text{ m}^2/\text{g}$) (Bag and Kanatzidis (2008; 2009; 2007; 2008)). High levels of iodine adsorption were demonstrated with the Ge-S-Pt chalcogels, both under high concentrations, i.e., a saturated iodine environment ($>240\%$ by mass), and low iodine concentrations ($>99\%$ by volume iodine sorption of available iodine). Both of these results are significant. Alternative chemistries were identified for the Ge-Ch-c gels including new precursors that should improve iodine sorption capacities – these include the substitution of Se for S and inclusion of Ag into the gel network. Also, a $\text{MoCo}_{0.5}\text{Ni}_{0.5}\text{S}_4$ hydrogel was successfully made and show promise as a lower cost replacement to the Ge-S-Pt gels.

1.1.2.10 Planned Improvements

Chalcogel scoping studies were performed with a Ge-S-Pt based chalcogel that are expensive. This system appeared to be a good starting point according the work of Bag *et al.* (2008; 2007) as the precursors are water soluble and relevant data was available. The most negative aspect of the Ge-Ch-Pt chemistries is the cost of the use of Pt as the catalyst. Other catalysts can be used in conjunction with Ge-Ch gels, i.e., Zn. After further literature review, alternate chemistries were studied and proposed for FY2011 and include (Mo,W)-S-(Ni,Co) and (Mo,W)-Se-(Ni,Co) systems, also studied by Bag *et al.*, (2009) which will reduce costs even further. We aim to investigate potentially chemistry changes that could improve the thermal stability of these chalcogels.

2. Metal Organic Frameworks for Xe and Kr immobilization

2.1 Key Personnel

Key Investigator: Praveen K. Thallapally
Key Contributors: Radha Motkuri, Satish Nune

Like zeolites, organic and metal-organic frameworks (MOFs) consist of open frameworks that can accommodate several different gas species. Different than zeolites, MOFs represent a new class of functional materials consisting of metal centers linked with organic building blocks to produce diverse and customizable structural frameworks (Thallapally et al. 2010; Thallapally et al. 2008). These metal centers and organic linkers readily self-assemble into

materials with open framework structures, where all the porosity is accessible for gas storage, separation and catalysis applications. Several porous materials (zeolites, activated carbons) were reported for gas storage applications but MOFs have received considerable attention over the past few years because of the high mass flux, thermal stability (in excess of 500°C for some MOFs), adjustable chemical functionalities and pore sizes, extra high porosity, and availability of hundreds of well characterized materials reminiscent to Zeolites (Figure 16). In addition, they readily grow as crystals of a different sizes suitable for gas separation technologies (e.g. to ca. 100 micrometre-size particles).

In this regard, over the past few months several metal organic frameworks were synthesized and characterized from Xe and Kr immobilization. The detailed synthesis and characterization of various MOFs for Kr immobilization are described below.

2.2 Synthesis and Characterization of MOF-5 (BDCZn):

One of the simplest of all the metal organic frameworks is based on benzenedicarboxylic acid (BDC) as organic building block and Zn₄O as inorganic connectors are joined to form an octahedral array of [O₂C-C₆H₄-CO₂]²⁻ groups to form a robust and highly porous cubic network (Figure 17). The scaffolding-like nature of MOF-5 and its derivatives leads to extraordinarily high apparent surface areas (2500 to 3000 m² g⁻¹) for these structures. On a practical level, the preparation of MOFs is simple, inexpensive, and of high yield. For example, the formation reaction for MOF-5 is

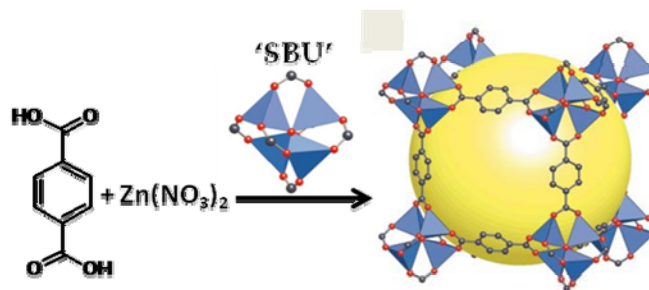


Figure 17. Synthesis and single crystal X-ray structure of MOF-5.

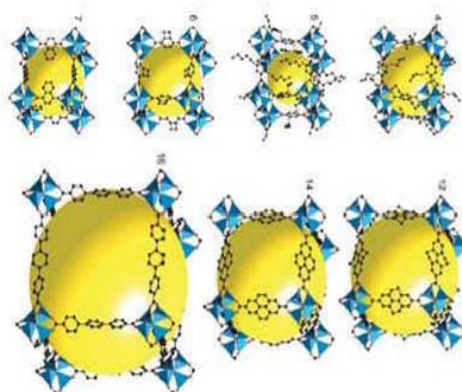
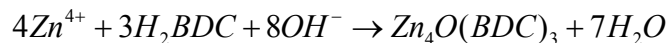


Figure 16. Metal-organic frameworks with different pore diameters (Rosi et al. 2003).



The MOF family also has high thermal stability with decomposition temperatures in the range of 300°C to 400°C. In this regard, we have successfully synthesized 500 mg of MOF-5 by dissolving $\text{Zn}(\text{NO}_3)_2 \cdot 6\text{H}_2\text{O}$ (350 mg) and BDC (60 mg) in 20 mL of dimethyl formamide solution at 100°C (Figure 17). After decanting the hot mother liquor, the product was washed with dimethylformamide (DMF) and dried in air for several hours. To produce the porous form of MOF-5, the resulting material was soaked overnight in 20 mL of chloroform solution for at least 2-3 times in 3 days to replace the trapped DMF. The trapped chloroform will be removed at high temperature under vacuum to get a porous MOF-5. Thermogravimetric analysis of the freshly synthesized MOF-5 shows 25 mass% loss from DMF in the host cavity (Figure 18). In order to know the thermal stability of MOF-5 before and after the solvent removal, *in-situ* powder X-ray diffraction was performed on a fresh sample under vacuum at room temperature and 200°C. The identical powder X-ray diffraction patterns (PXRDs) of MOF-5 confirms the structural stability and porous nature of the synthesized material (Figure 19). The gas adsorption experiments were performed on this sample with our HPA-100 volumetric gas analyzer and Intelligent Gravimetric Analyzer (IGA-100) as described in the Section 2.4.

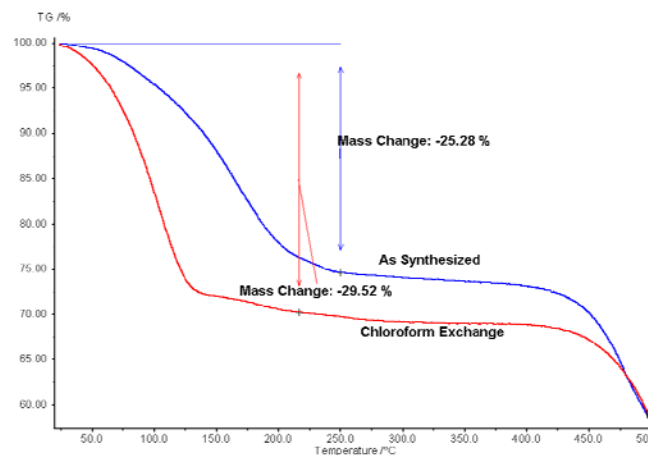


Figure 18. Thermal analysis of as synthesized MOF-5 and DMF exchanged with chloroform.

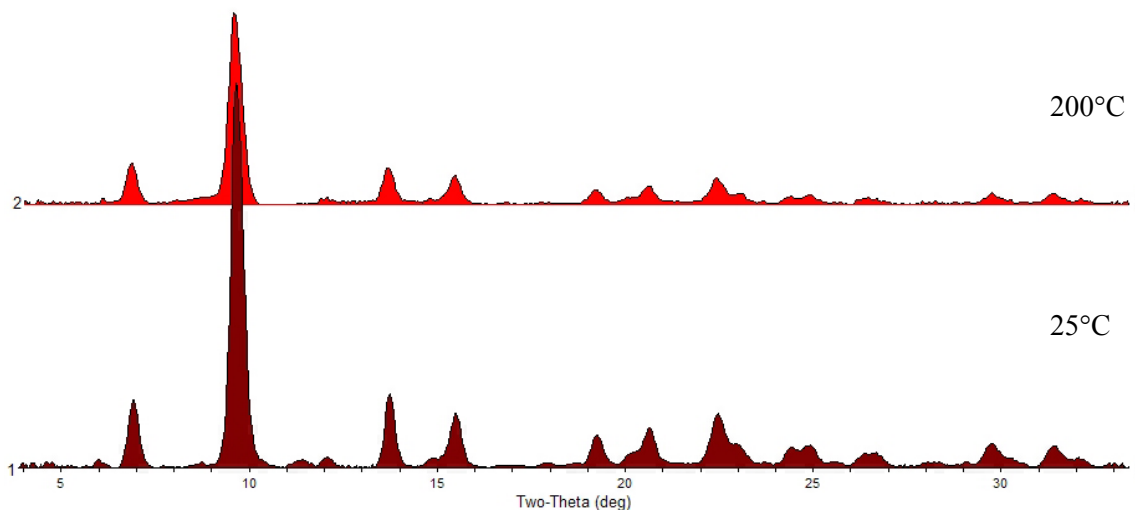


Figure 19. In-situ Powder X-ray diffraction of MOF-5 at room 25°C and 200°C under vacuum.

2.3 Synthesis and Characterization of DHTANi:

Along with MOF-5, we have synthesized and characterized 2,5-dihydroxy terephthalic acid-Ni (DHTANi) MOF, which shows an outstanding uptake and selectivity towards CO₂ over nitrogen gas. Therefore DHTANi was prepared by heating a DMF solution containing

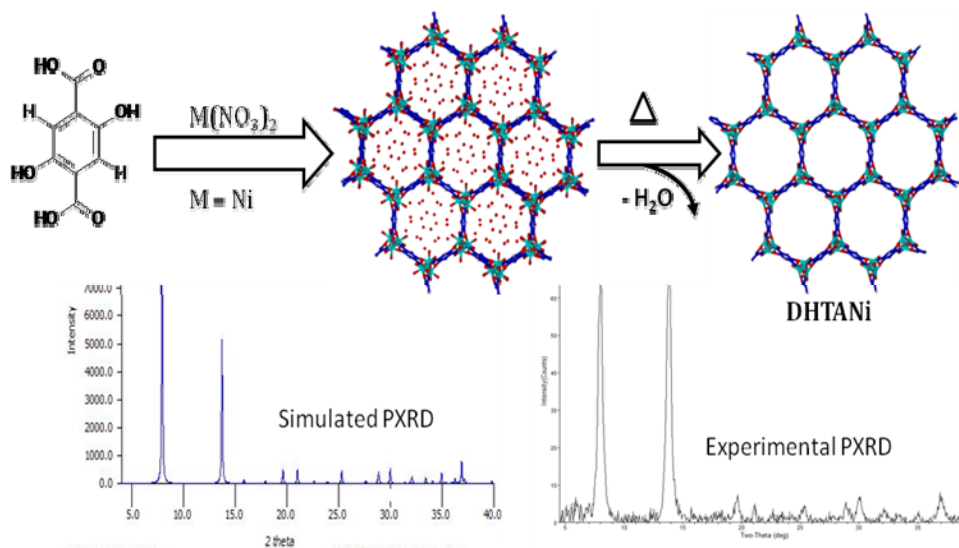


Figure 20. Synthesis and structural topology of DHTANi.

DHTA and nickel nitrate for 10 h at 100°C. The resulting precipitate was filtered and characterized further to obtain the porosity and thermal stability. The DHTANi contains a three dimensional honeycomb-like network structure, with a large one-dimensional cylindrical channel having a diameter about 1.1 nm (Figure 20). The metal sites in the framework are unsaturated following the removal of coordinated solvent molecules from the framework, which is expected to give exceptionally strong binding with solutes. Moreover, DHTANi has a very large pore volume, which should allow the sorption of large quantities of gas at relatively low pressures. With these two promising properties, strong solute interactions and a high pore volume, DHTANi shows promising attributes to be an effective material for the immobilization of Kr, Xe, and other gases. As shown in Figure 20, the simulated and experimental PXRD are identical confirming successful synthesis of DHTANi without any impurities. Thermogravimetric analysis coupled with mass spectra of DHTANi shows 25 to 30 mass% loss between room temperature and 250°C, which corresponds to the loss of trapped water molecules as suggested by

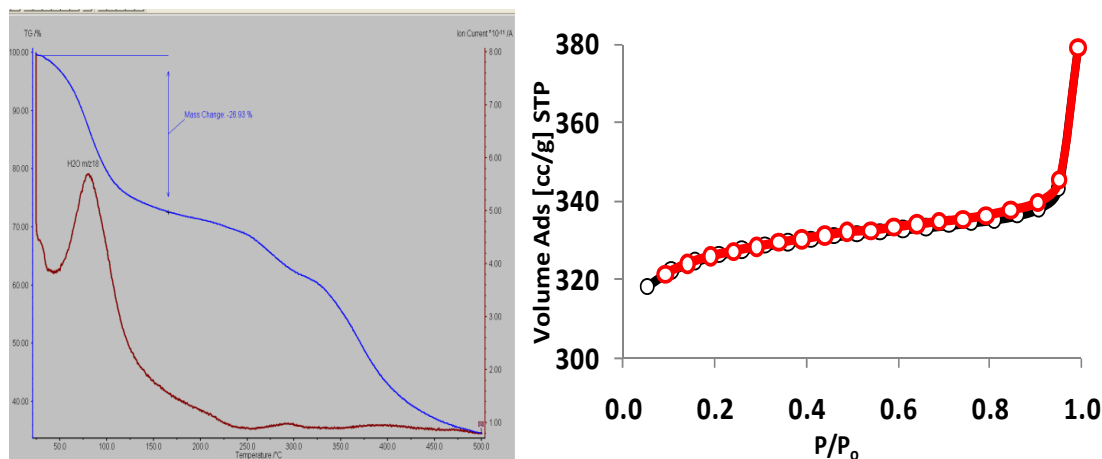


Figure 21. TG-MS and BET surface area measurements on DHTANi.

the mass-to-atomic number ratio of 44 (Figure 21). Prior to the sorption studies, the surface area of the activated sample was calculated from the N_2 adsorption at 77 K, which exhibits a typical Type I isotherm with surface area of $980 \text{ m}^2 \text{ g}^{-1}$ suggesting porous nature of DHTANi (Figure 21).

2.4 Xenon and Kr measurements using HPVA-100 and IGA-100

The gas adsorption experiments were performed on all the activated materials with our two analyzers as shown in Figure 22. Gas sorption experiments with Xe and Kr were performed at room temperature. Both MOF-5 and DHTANi were placed in a sample chamber separately, and activated at high temperature under vacuum for several hours. For low pressure experiments, the adsorbate (Xe or Kr) at 10 kPa was dosed into the sample chamber every 10 min, and the volume adsorbed per gram of material was plotted against the pressure. At this pressure (100 kPa) the calculated mass change was found to be close to 30 mass% of Xe and 40 wt% of Kr. Similarly, DHTANi shows an uptake of 55 mass% of Xenon at room temperature (Figure 23), which is higher than any other solid sorbent reported thus far for Xe. The absence of hysteresis during desorption of these gases is not surprising, and it has been found to be very common for materials with a pore size of 2 nm or less. The measurements were repeated several times by evacuating the sample and pressurizing with adsorbate again. The same mass changes were obtained within $\pm 5\%$.

2.5 Air Stable Zeolitic Imidazolate Framework (ZIF) for Kr Immobilization:

One of the drawback with metal organic frameworks include the adsorption of water vapor. To address this problem many research groups, including us, are functionalizing these materials with hydrophobic groups to increase the contact angle. In this regard, previous studies on zeolitic imidazolate frameworks, particularly ZIF-8, a sub class of metal organic frameworks, by us and others (Nune et al. 2010) for use in CO_2 capture found that this material is robust and does not react with water. Experiments with this material showed that it does not decompose in N_2 up to 600°C . This material is made by heating the DMF solution containing ZIF and zinc nitrate hexahydrate at 110°C . Freshly synthesized ZIF-8 was soaked in a methanol solution for 3 d to 10 d to remove the DMF from the pores of ZIF-8. The identical PXRD indicate similar network topology after soaking in methanol solution. The same sample was



Figure 22. High pressure volumetric gas analyzer (HPVA-100, Left) and low pressure gravimetric gas analyzer coupled with MS and Breakthrough reactor (IGA-100, Right).

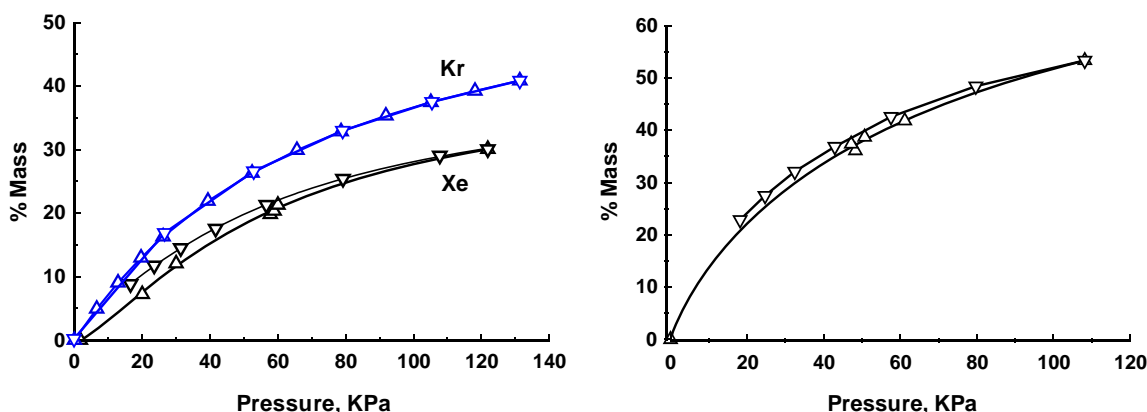


Figure 23. Xenon and Kr adsorption (Δ) and desorption (∇) kinetics in MOF-5 (Left) and DHTANi (Right) at 25°C.

heated under vacuum at 220°C to remove the trapped solvent molecules, the identical PXRD indicate the structural stability and porosity without solvent molecules. Similarly, a fresh as-synthesized ZIF-8 was heated at 220°C in air to determine the stability in air. Figure 25 shows the stability of ZIF-8 in air. The shifted low 2θ peaks could be explained by the slight framework contraction. Overall ZIF-8 is thermally stable when heated in air (Figure 24).

2.6 Conclusions and Future Studies

In conclusion, several MOFs were synthesized and characterized. The results show that MOFs have a large capacity for Xe at relatively low pressure with reversible adsorption and desorption of Xe. The same results are expected for Kr. Future studies will be focused around MOFs discussed above for Kr adsorption experiments at various temperatures and low partial pressures. Larger test quantities of these materials will be made to perform Kr breakthrough experiments on the intelligent thermogravimetric analyzer. Similarly we will explore the use of these materials for Iodine removal. Although not an active part of this program, we and other researchers (Zeng et al. 2010) have explored these novel materials for removal I_2 and have been found to incorporate 60 to 100 mass% I_2 inside the cavities (Figure 25 from Zeng et. al., 2010). During this process the crystals change color less to colored materials.

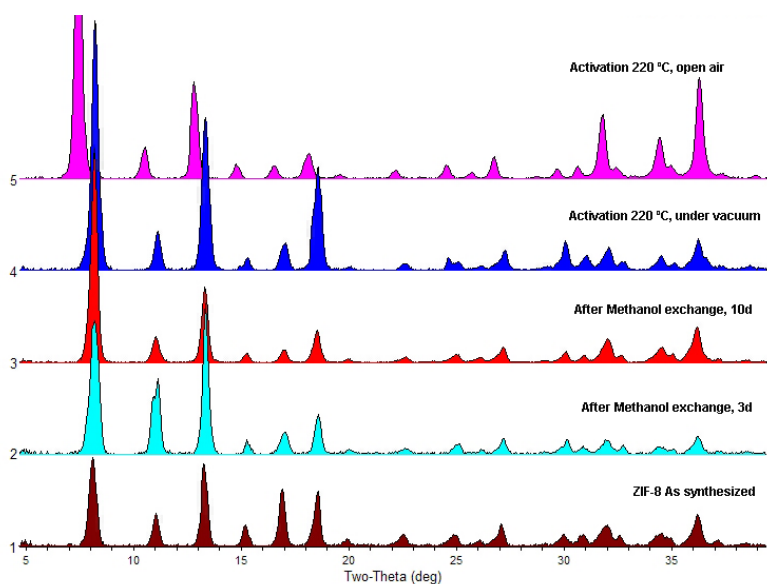


Figure 24. Structural stability of ZIF-8 under vacuum and air.

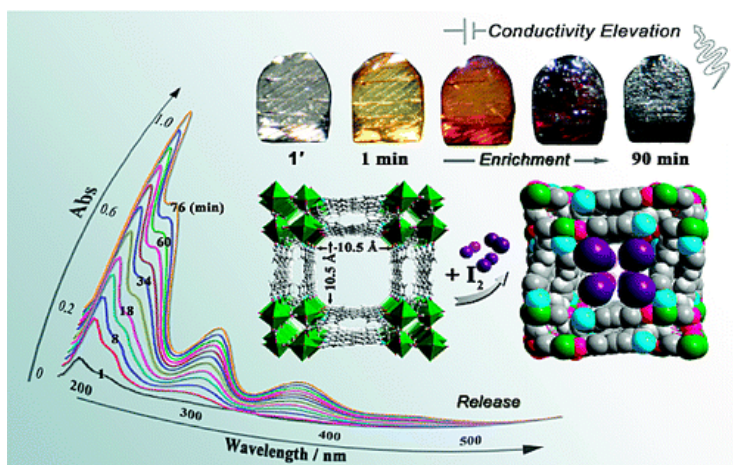


Figure 25. Metal Organic Frameworks suitable for Iodine adsorption.

3. Silicon Carbide for Gaseous Radionuclide Immobilization

3.1 Key Personnel

Charles H. Henager, Jr; Joseph V. Ryan; Wendy Bennett; Charles C. Bonham

3.2 Background

Because of the low diffusivities for fission products and superior physical and chemical stability of silicon carbide (SiC), it is an ideal candidate for immobilization of C, Kr, and Xe (and perhaps other fission products). Silicon carbide possesses excellent physical and chemical properties that make it a promising material, not only for advanced electronic devices (Raynaud 2001), but also for structural components in fusion reactors (Fenici et al. 1998; Nogami et al. 2009; Zhao et al. 2007; Wong et al. 2007; Katoh et al. 2007), a barrier for fission product diffusion in gas-cooled fission reactors (Kim et al. 2000), and an inert matrix for the transmutation of plutonium and other transuranics (Verrall, Vlajic and Krstic 1999; Krstic, Vlajic and Verrall 1996). The high thermal conductivity of SiC also enhances homogeneous heat distribution in devices and rapid heat transfer. Unlike traditional semiconductor materials, thermal diffusion of dopants in SiC requires extremely high temperatures because of the extremely low diffusivities for impurities in SiC. This low diffusivity for impurities is one of the reasons SiC is used as the fission product barrier in tri-structural-isotropic (TRISO) nuclear fuel and its use for this application has been demonstrated at temperatures over 2000 K (Schenk and Nabielek 1991; Schenk, Pott and Nabielek 1990; Nabielek et al. 1990). Because of the low diffusivities for fission products and superior physical and chemical stability of SiC, it is an ideal candidate for immobilization of C, Kr, and Xe (and perhaps other fission products). Thermal release of helium generated in neutron-irradiated SiC does not occur until temperatures above 1200 K (Sasaki et al. 1991; Sasaki, Maruyama and Iseki 1989). Because of its low chemical reactivity, SiC is also proposed as cladding for advanced light water reactors (Filippov et al. "Computational Estimate of the Corrosion Resistance of Fuel Microelements with Silicon Carbide Cladding in a Water Medium at Supercritical Pressure" 2007; Filippov et al. "Erratum: Computational Estimate of the Corrosion Resistance of Fuel Microelements with Silicon Carbide Cladding in a Water Medium at Supercritical Pressure (Atomic Energy (2007) 102:3 (204-210) Doi: 10.1007/S10512-007-0030-2)" 2007; Filippov et al. 2006). A recent discovery of pitting corrosion in β -SiC at 300°C, however, indicates that even this stable material is not immune to low-temperature corrosion involving volatile SiOH species (Henager Jr et al. 2008). Although pits were observed in this study no measurable mass loss occurred for exposure times up to 4000 hours. While oxidation of SiC occurs at elevated temperatures, such oxide films generally form a barrier to further oxidation and should be negligible under conditions for immobilization unless significant water vapor is present (Opila 2003). Silicon carbide also occurs in nature as the extremely rare mineral moissanite (Bauer, Fiala and Hrichova 1963; Pierro et al. 2003), and SiC crystals of interstellar origin have been found in primitive meteorites (Alexander, Swan and Walker 1990), both of which support its physical and chemical stability.

Since industrial scale fabrication of SiC monoliths with physical vapor deposition methods is a well-established technology (Abe et al. 2008; Jiangang et al. 2006; Sadow et al. 2001; Moon et al. 2001; Sugiyama et al. 1998), there is little, if any, technology development needed to produce dense, pure SiC. While there are many polymorphs of SiC, the cubic 3C structure is preferred for nuclear and structural applications, such as ceramic composite fibers and matrices and fine-grained coatings for TRISO nuclear fuel particles. Much of our knowledge of diffusivities of nuclear isotopes in SiC comes from studies of TRISO fuel particles (Peterson and Dunzik-Gougar 2006; Schenk, Naoumidis and Nickel 1984; Smith 1979; Fukuda and Iwamoto 1978; Fukuda and Iwamoto 1976; Fukuda and Iwamoto 1975). Studies have shown that Xe and Kr have extremely low mobilities in SiC at low temperatures and only become mobile above 1200°C (Fukuda and Iwamoto 1978; Fukuda and Iwamoto 1976; Fukuda and Iwamoto 1975).

Thus, it appears that SiC is almost an ideal candidate material for storage and retention of radioactive C, Xe, and Kr.

For immobilization of fission products, physical vapor deposition of monolithic 3C-SiC provides an industrial scale process from which to begin this development. It was anticipated that optimized physical vapor deposition (PVD) or chemical vapor deposition (CVD) technology with ion-assisted deposition would allow the synthesis of a SiC waste form with entrained radioactive C, Xe, and/or Kr. Captured carbon from reprocessing could supplement the carbon source used in processing, typically in the form of methyltrichlorosilane, CH_3SiCl_3 (Jiangang et al. 2006). Gaseous fission products, such as Xe and Kr, could be injected onto the surface with low energy ion guns or leaked into processing chamber (Grigorov and Martev 1988). One prior study indicated that up to 20 atomic % Ar could be entrained during PVD of Ti-films (Grigorov and Martev 1988). It is anticipated that equivalent amounts for Xe and Kr could be entrained within CVD or PVD SiC. Since Xe and Kr diffusivities are extremely low at ambient temperatures, the release rates of Xe and Kr are negligible, even along grain boundaries, for millions of years (Sauvage et al. 2007; Van Ginhoven et al. 2006; Pramono, Sasaki and Yano 2004; Chen, Jung and Trinkaus 2000; Jung 1992; Fukuda and Iwamoto 1978; Fukuda and Iwamoto 1976).

3.3 Experimental Methods and Materials

A SiC target was obtained and a 0.7-m box coating chamber was outfitted for deposition with a 75 mm-inch Mity Mak magnetron sputtering cathode. Deliverable coatings were deposited on 2 inch diameter polished Si substrates or ~10 mm square NaCl crystals. Silicon substrates were mounted in the center of a stainless steel-foiled substrate holder using clips. The NaCl crystals were mounted on carbon tape with the addition of a stainless steel mesh to prevent the crystals from falling off during deposition. An anti-stat N_2 gun was used to blow off debris prior to loading in the coating chamber. Table 2 contains the experimental configurations used in these experiments.

To reduce arcing and debris generation during the ion-assisted depositions, stainless steel foil was mounted on the interior right side of the coating chamber closest to the ion gun. Stainless steel foil was also used to cover the substrate holder and surround the exterior of the unbalanced magnetron (UBM) cathode. The substrate was rotated directly over the target. A single leaf shutter was positioned between the target and the substrate to mask the substrate during target cleaning prior to the start of each deposition. It was then rotated toward the rear of the chamber to allow disposition on the substrate. For depositions using the 3" SiC target, the spacing between the substrate and the target was 5 inches. A DynaVac IS1000 gridless, end-Hall type ion source was used for most of the krypton deposition, powered by an MDX Advanced Energy power supply. The ion gun was angled 30 deg toward the cathode/substrate (Figure 26) such that the ion flux would be co-incident with the primary ad-atom flux at the substrate material. For depositions using the UBM, the substrate/target gap was 3.5 inches, which is the optimum range of the UBM field. Fig 4 shows the initial setup using the UBM; it was later optimized for better ion-assist by rotating the UBM 90-deg and positioning the ion gun as used with the 3" depositions. Unfortunately, no photos were taken.

An overnight pump-down was critical to reaching an ultimate chamber pressure of low 1.3×10^{-5} or mid 1.3×10^{-6} Pa. The 75 mm SiC depositions were performed at a pressure of ~0.5 Pa and $0.017 \text{ m}^3/\text{s}$ of either 100% Ar or Kr. They utilized an RF -10 power supply and in-house built matching network operating at 200W and ~220-240V for non-ion assist depositions. During the ion-assist depositions, the voltage dropped to 130-170V for the same 200W input due to interference from the ion gun. The ion gun neutralizer was set at ~19V and 35A to reduce arcing. The ion gun drive was set at either 0.05kW/120V (reduced cathode voltage to 150-170V) or 0.1kW/116V (reduced cathode voltage to 130-150V). The deposition time for 1 micron of either non-ion assist or IAD was 3 hr and 20-25min.

The UBM depositions utilized a PE 5000 AC Plasma power supply operating at 0.5kW/0.75A and ~700V for non-ion assist depositions. During IAD, the parameters were 0.3kW/0.5A and ~580V. A 1- μm SiC

Table 2. Experimental Setup for the SiC experiments.

Run #	Substrate	non-IAD	IAD	75 mm Cathode	UBM
Setup: substrate directly over 75 mm cathode, ion gun 30 degrees toward cathode					
1G-S	5mm Si	X		X	
1I-S	5mm Si	X		X	
1K-S	5mm Si	X	X	X	
1L-S	5mm Si	X	X	X	
Setup: substrate directly over UBM cathode; PE 5000 AC power supply					
2G-S	5mm Si	X	X		X
Setup: substrate directly over UBM cathode, PE 5000 AC power supply, ion gun and cathode positioned as shown in Figure 3					
2I-S	5mm Si	X	X		X
Setup: UBM cathode rotated 90 degrees, substrate directly over cathode; PE 5000 AC power supply; ion gun positioned directly in front of cathode					
2J-S	NaCl		X		X

deposition took ~ 3 h. The ion gun parameter for the UBM depositions were: neutralizer was 11.2V/10A; drive was 0.1kW/215V.

Calibration runs were performed to determine the SiC deposition rate for a bonded SiC target with and without ion assist. The goal of the calibrations was to determine the substrate positioning that gave us the most uniform and highest deposition rate.



Figure 26. Initial ion gun deposition setup for SiC immobilization experiments with Kr.

3.4 Results

The initial deliverable depositions consisted of two coating structures, each with two approximately one micrometer thick layers. The first consisted of SiC deposited in a 100% Ar atmosphere capped by

SiC deposited in a 100% Kr atmosphere. The second film consisted of the same argon-deposited base layer, but with the top deposition including Kr applied with the ion source. In this top layer, Kr was also the deposition gas with no argon used. Following these depositions, we also attempted several depositions using UBM sputtering. In these cases, the ion gun was used, but may not have had much of an effect due to the short working distance necessary to produce the films.

Three films were analyzed using a VersaProbe XPS system through the Environmental and Molecular Sciences Laboratory user facility on the PNNL campus. Each sample exhibited a similar C/Si atomic ratio, slightly enriched in C over a pure SiC stoichiometry. This was expected, as the target SiC material used (Saint Gobain SG-90) is also C enriched by several atomic percent to maintain conductivity and thus good sputtering

behavior. Also in each case, the surface concentration of Kr was slightly higher than the bulk as seen in Figure 2. Resolving the reasons for this occurrence is one of the goals of the ongoing research. It may be due to the Ar ion used to mill the film surface away to achieve the depth profile or it may be a true compositional gradient. Further Ar milling and time spent under the ultra-high vacuum of the XPS instrument did not appreciably change the elemental composition of any of the films. In any event, the transient surface composition was not used for comparative purposes in preference of the more stable composition established with a 2 minute 2 kV Ar beam mill.

As expected, Sample 1I-S exhibited the lowest concentration of Kr of the three samples at 1.4 atomic percent (or 4.4 mass percent). The incorporation of sputtering ions into films is typically minimal due to the fact that most of the ion energy is taken up in the sputtering process. Trapping mechanisms and some bias-resputtering are typically thought to account for this low-level incorporation. The addition of Kr through an energetic ion source, however, produced dramatically different results. In this case (sample 1L-S), 6.7 atomic percent (or 21.6 mass percent) of Kr was incorporated into the bulk of the sample. The sample deposited with UBM exhibited similar results, with 5.6 atomic percent (18.0 mass percent) Kr incorporated into the film. This result is interesting because it was difficult to impinge the ion stream onto the growing film. With a more favorable geometry, this may indeed represent the most successful option.

3.5 Future Work

A small ion implantation system (Peabody Scientific Ion Implanter System) has been made available to the project and is currently being installed on the PVD chamber where the previous sputter depositions were performed, as shown in Figure 4. We plan to repeat the earlier IAD runs without the small ion gun but with the ion implanter system operating at about 5 keV for the first depositions, with the ion energy gradually increased in subsequent runs up to 40keV, which is the maximum achievable with this system. Further, the SiC films containing Kr will be deposited on NaCl crystals and so that the NaCl can be

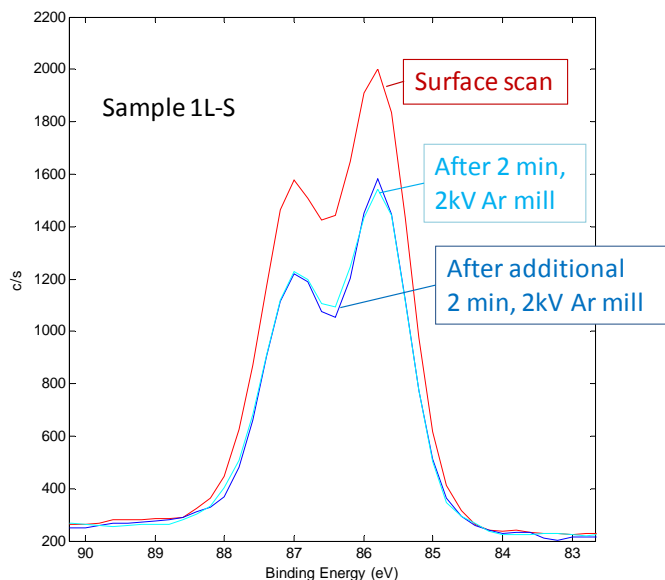


Figure 27. X-ray photoelectron spectra of the Kr 3d region showing Kr immobilized in sputtered SiC. This sample exhibited the maximum retention of 6.7 atomic % Kr (21.6 mass %).

dissolved leaving behind Kr-loaded SiC. We can determine the amount and rate of release of Kr in the IGA-100 gas desorption with increasing temperature.



Figure 28. Unbalanced magnetron setup used for several Kr immobilization experiments.



Figure 29. Peabody Scientific Ion Implanter System with beam energy: 2 to 40 keV via a Duoplasmatron Ion Source and low-pressure arc discharge system.

4. References

- Abe, K, Y Nagasaka, T Kida, T Yamakami, R Hayashibe, and K Kamimura. 2008, "Characterization of Polycrystalline SiC Films Grown by HW-CVD Using Silicon Tetrafluoride." *Thin Solid Films* 516:637-40.
- Alexander, CMOD, P Swan, and RM Walker. 1990, "In Situ Measurement of Interstellar Silicon Carbide in Two Cm Chondrite Meteorites." *Nature* 348:715-17.
- Bag, S, IU Arachchige, and MG Kanatzidis. 2008, "Aerogels from Metal Chalcogenides and Their Emerging Unique Properties." *Journal of Materials Chemistry* 18:3628-32.
- Bag, S, AF Gaudette, ME Bussell, and MG Kanatzidis. 2009, "Spongy Chalcogels of Non-Platinum Metals Act as Effective Hydrodesulfurization Catalysts." *Nature Chemistry* 1:217-24.
- Bag, S, PN Trikalitis, PJ Chupas, GS Armatas, and MG Kanatzidis. 2007, "Porous Semiconducting Gels and Aerogels from Chalcogenide Clusters." *Science* 317:490-93.
- Bauer, J, J Fiala, and R Hrichova. 1963, "Natural -Silicon Carbide." *American Mineralogist* 48:620-34.
- Bowes, CL, WU Huynh, SJ Kirkby, A Malek, GA Ozin, S Petrov, M Twardowski, and D Young. 1996, "Dimetal Linked Open Frameworks: $[(CH_3)_4N]_2(Ag_2Cu_2)Ge_4S_{10}$." *Chemistry of Materials* 8:2147-52.
- Brock, SL. 2007, "Filling a Void." *Science* 317:460-61.
- Chen, J, P Jung, and H Trinkaus. 2000, "Microstructural Evolution of Helium-Implanted -SiC." *Physical Review B (Condensed Matter)* 61:12923-32.
- CRC Handbook of Chemistry and Physics. 2007-2008. 88th ed., CRC Press, Boca Raton, FL.
- Fenici, P, AJF Rebelo, RH Jones, A Kohyama, and LL Snead. 1998, "Current Status of SiC/SiC Composites R&D." *Journal of Nuclear Materials* 258-263:215-25.
- Filippov, GA, EI Grishanin, MV Konditerov, VP Mastuykin, VI Mel'kin, VM Trubachev, LN Fal'kovskii, BI Fonarev, and GV Momot. 2006, "Investigation of the Corrosion Resistance of Fuel Micropellet Cladding Made of Silicon Carbide and Pyrolytic Carbon for the Operating Conditions of Light-Water Reactors in Nuclear Power Plants." *Atomic Energy* 101:722-29.
- Filippov, GA, EI Grishanin, YE Lebedev, VM Trubachev, LN Fal'Kovskii, and BI Fonarev. 2007, "Computational Estimate of the Corrosion Resistance of Fuel Microelements with Silicon Carbide Cladding in a Water Medium at Supercritical Pressure." *Atomic Energy* 102:204-10.
- Filippov, GA, EI Grishanin, YE Lebedev, VM Trubachev, LN Fal'kovskii, and BI Fonarev. 2007, "Erratum: Computational Estimate of the Corrosion Resistance of Fuel Microelements with Silicon Carbide Cladding in a Water Medium at Supercritical Pressure (*Atomic Energy* (2007) 102:3 (204-210) Doi: 10.1007/S10512-007-0030-2)." *Atomic Energy* 102:329.

Fukuda, K, and K Iwamoto. 1975, "Diffusion and Evaporation of Fission Products in Coated Fuel Particles." *Journal of Nuclear Science and Technology* 12:181-9.

Fukuda, K, and K Iwamoto. 1978, "Diffusion Behavior of Fission Product in Pyrolytic Silicon Carbide." *Journal of Nuclear Materials* 75:131-44.

Fukuda, K, and K Iwamoto. 1976, "Xenon Diffusion Behaviour in Pyrolytic SiC. [Coating Material for Nuclear Fuel Particles]." *Journal of Materials Science* 11:522-8.

Gombert II, D. 2007, Global Nuclear Energy Partnership Integrated Waste Management Strategy Waste Treatment Baseline Study, Volume I. Technical Rpt. GNEP-WAST-AI-RT-2007-000324, Idaho National Laboratory, Idaho Falls, ID.

Grigorov, GI, and IN Martev. 1988, "Inert Gas Entrapment in Films Produced by Ion-Assisted Physical Vapour Deposition Processes." *Thin Solid Films* 156:265-9.

Henager Jr, CH, AL Schemer-Kohrn, SG Pitman, DJ Senor, KJ Geelhood, and CL Painter. 2008, "Pitting Corrosion in CVD SiC at 300°C in Deoxygenated High-Purity Water." *Journal of Nuclear Materials* 378:9-16.

Hilton, AR, and DJ Hayes. 1975, "The Interdependence of Physical Parameters for Infrared Transmitting Glasses." *Journal of Non-Crystalline Solids* 17:339-48.

Jiangang, D, N Singh, JB Summers, and CA Zorman. 2006, "Development of Pecvd SiC for Mems Using 3ms as the Precursor." in *Silicon Carbide 2006-Materials, Processing and Devices. Symposium*, ed. MRS, Vol *Silicon Carbide 2006-Materials, Processing and Devices. Symposium (MRS Proceedings Vol. 911)*, pp. 283-8. Materials Research Society, San Francisco, CA, USA.

Jung, P. 1992, "Diffusion and Retention of Helium in Graphite and Silicon Carbide." *Journal of Nuclear Materials* 191-94:377-81.

Kanatzidis, MG, and S Bag. 2008, "Semiconducting Aerogels from Chalcogenido Clusters With Broad Applications." USA.

Kasper, JS, and SM Richards. 1964, "The Crystal Structures of New Forms of Silicon and Germanium." *Acta Crystallographica* 17:752-55.

Katoh, Y, LL Snead, CH Henager Jr, A Hasegawa, A Kohyama, B Riccardi, and H Hegeman. 2007, "Current Status and Critical Issues for Development of SiC Composites for Fusion Applications." *Journal of Nuclear Materials* 367-370 A:659-71.

Kim, BG, Y Choi, JW Lee, YW Lee, DS Sohn, and GM Kim. 2000, "Multi-Layer Coating of Silicon Carbide and Pyrolytic Carbon on UO₂ Pellets by a Combustion Reaction." *Journal of Nuclear Materials* 281:163-70.

Kirilenko, VV, and SA Dembovskii. 1975, "Glass Formation and Chemical Compounds in the Systems A(IV)-B(VI)-C(VII) (A(IV)=Si, Ge; B(VI)=S, Se; C(VII)=Br, I) (in Russian)." *Fizika i Khimiya Stekla* 1:225-29.

Krstic, VD, MD Vlajic, and RA Verrall. 1996, "Silicon Carbide Ceramics for Nuclear Application." *Key Engineering Materials* 122-124:387-96.

- Liu, L-G, WA Bassett, and J Sharry. 1978, "New High-Pressure Modifications of GeO₂ and SiO₂." *Journal of Geophysical Research* 83:2301-05.
- Moon, CK, HJ Song, JK Kim, JH Park, SJ Jang, JB Yoo, HR Park, and B-T Lee. 2001, "Chemical-Vapor-Deposition Growth and Characterization of Epitaxial 3c- SiC Films on Soi Substrates with Thin Silicon Top Layers." *Journal of Materials Research* 16:24-27.
- Nabielek, H, W Kuhnlein, W Schenk, W Heit, A Christ, and H Ragoss. 1990, "Development of Advanced HTR Fuel Elements." *Nuclear Engineering and Design* 121:199-210.
- Nogami, S, A Hasegawa, T Murayama, N Otake, M Satou, and K Abe. 2009, "Compatibility between SiC and Li Ceramics for Solid Breeding Blanket System." *Journal of Nuclear Materials* 386-388:628-30.
- Nune, SK, PK Thallapally, A Dohnalkova, CM Wang, J Liu, and GJ Exarhos. 2010, "Synthesis and Properties of Nano Zeolitic Imidazolate Frameworks." *Chemical Communications* 46:4878-80.
- Opila, EJ. 2003, "Oxidation and Volatilization of Silica Formers in Water Vapor." *Journal of the American Ceramic Society* 86:1238-48.
- Pearson, RG. 1963, "Hard and Soft Acids and Bases." *Journal of the American Chemical Society* 85:3533-39.
- Peterson, J, and ML Dunzik-Gougar. 2006, "Degradation of Triso Fuel in a Repository Environment." *Transactions of the American Nuclear Society* 94:668-9.
- Pierro, SD, E Gnos, BH Grobety, T Armbruster, SM Bernasconi, and P Ulmer. 2003, "Rock-Forming Moissanite (Natural A-Silicon Carbide)." *American Mineralogist* 88:1817-21.
- Pivan, JY, O Achak, M Louër, and D Louër. 1994, "The Novel Thiogermanate [(CH₃)₄N]₄Ge₄S₁₀ with a High Cubic Cell Volume. Ab Initio Structure Determination from Conventional X-Ray Powder Diffraction." *Chemistry of Materials* 6:827-30.
- Pramono, Y, K Sasaki, and T Yano. 2004, "Release and Diffusion Rate of Helium in Neutron-Irradiated SiC." *Journal of Nuclear Science and Technology* 41:751-55.
- Raynaud, C. 2001, "Silica Films on Silicon Carbide: A Review of Electrical Properties and Device Applications." *Journal of Non-Crystalline Solids* 280:1-31.
- Riley, B, S Sundaram, BR Johnson, and LV Saraf. 2008, "Differential Etching of Chalcogenides for Infrared Photonic Waveguide Structures." *Journal of Non-Crystalline Solids* 354:813-16.
- Rosi, NL, J Eckert, M Eddaoudi, DT Vodak, J Kim, M O'Keeffe, and OM Yaghi. 2003, "Hydrogen Storage in Microporous Metal-Organic Frameworks." *Science* 300:1127-29.
- Ryan, J, E Buck, J Chun, J Crum, B Riley, D Strachan, S Sundaram, L Turo, and J Vienna. 2009, *Alternate Waste Forms: Aqueous Processing*. Technical, PNNL, Richland, WA.
- Saddow, SE, TE Schattner, J Brown, L Grazulis, K Mahalingam, G Landis, R Bertke, and WC Mitchel. 2001, "Effects of Substrate Surface Preparation on Chemical Vapor Deposition Growth of 4h- SiC Epitaxial Layers." *Journal of Electronic Materials* 30:228-34.

Sasaki, K, T Maruyama, and T Iseki. 1989, "Helium Release from Neutron-Irradiated SiC Containing 10b Isotope." *Journal of Nuclear Materials* 168:349-51.

Sasaki, K, T Yano, T Maruyama, and T Iseki. 1991, "Helium Release and Microstructure of Neutron-Irradiated SiC Ceramics." Vol 179-181, pp. 407-10, Netherlands.

Sauvage, T, G Carlot, G Martin, L Vincent, P Garcia, MF Barthe, A Gentils, and P Desgardin. 2007, "Helium Behavior in -SiC Ceramics Investigated by NRA Technique." *Nuclear Instruments and Methods in Physics Research, Section B: Beam Interactions with Materials and Atoms* 257:231-35.

Schenk, W, and H Nabielek. 1991, "High-Temperature Reactor Fuel Fission Product Release and Distribution at 1600 to 1800C." *Nuclear Technology* 96:323-36.

Schenk, W, A Naoumidis, and H Nickel. 1984, "Behaviour of Spherical HTR Fuel Elements under Accident Conditions." *Journal of Nuclear Materials* 124:25-32.

Schenk, W, G Pott, and H Nabielek. 1990, "Fuel Accident Performance Testing for Small HTRs." *Journal of Nuclear Materials* 171:19-30.

Smith, CL. 1979, "SiC-Fission Product Reactions in HTGR Triso UC2 and UCxOy Fissile Fuel. II. Reactions under Isothermal Conditions." *Journal of the American Ceramic Society* 62:607-13.

Smith, GS, and PB Isaacs. 1964, "The Crystal Structure of Quartz-Like GeO₂." *Acta Crystallographica* 17:842-46.

Strachan, DM, SA Bryan, CH Henager, TG Levitskaia, J Matyas, PK Thallapally, RD Scheele, WJ Weber, and F Zheng. 2009, Processes for Removal and Immobilization of ¹⁴C, ¹²⁹I, and ⁸⁵Kr. Technical Rpt. PNNL-18852, Pacific Northwest National Laboratory, Richland, WA.

Sugiyama, N, A Okamoto, K Okumura, T Tani, and N Kamiya. 1998, "Step Structures and Dislocations of SiC Single Crystals Grown by Modified Lely Method." *Journal of Crystal Growth* 191:84-91.

Thallapally, PK, RK Motkuri, CA Fernandez, BP McGrail, and GS Behrooz. 2010, "Prussian Blue Analogues for CO₂ and SO₂ Capture and Separation Applications." *Inorganic Chemistry* 49:4909-15.

Thallapally, PK, J Tian, MR Kishan, CA Fernandez, SJ Dalgarno, PB McGrail, JE Warren, and JL Atwood. 2008, "Flexible (Breathing) Interpenetrated Metal-Organic Frameworks for CO₂ Separation Applications." *Journal of the American Chemical Society* 130:16842-+.

Van Ginhoven, RM, A Chartier, C Meis, WJ Weber, and LR Corrales. 2006, "Theoretical Study of Helium Insertion and Diffusion in 3c-SiC." *Journal of Nuclear Materials* 348:51-59.

Verrall, RA, MD Vljajic, and VD Krstic. 1999, "Silicon Carbide as an Inert-Matrix for a Thermal Reactor Fuel." *Journal of Nuclear Materials* 274:54-60.

Wei, T-Y, T-F Chang, S-Y Lu, and Y-C Chang. 2007, "Preparation of Monolithic Silica Aerogel of Low Thermal Conductivity by Ambient Pressure Drying." *Journal of the American Ceramic Society* 90:2003-07.

Wong, CPC, V Chernov, A Kimura, Y Katoh, N Morley, T Muroga, KW Song, YC Wu, and M Zmitko. 2007, "ITER-Test Blanket Module Functional Materials." *Journal of Nuclear Materials* 367-370:1287-92.

Zeng, MH, QX Wang, YX Tan, S Hu, HX Zhao, LS Long, and M Kurmoo. 2010, "Rigid Pillars and Double Walls in a Porous Metal-Organic Framework: Single-Crystal to Single-Crystal, Controlled Uptake and Release of Iodine and Electrical Conductivity." *Journal of the American Chemical Society* 132:2561-+.

Zhao, J, G Wang, Q Guo, and L Liu. 2007, "Microstructure and Property of SiC Coating for Carbon Materials." *Fusion Engineering and Design* 82:363-68.